ISTANBUL TECHNICAL UNIVERSITY ★ GRADUATE SCHOOL

IMAGE PROCESSING SOFTWARE TOOLS DEVELOPMENT FOR SHOULDER ARTHROPLASTY

Ph.D. THESIS

Majid MOHAMMAD SADEGHI

Department of Mechatronics Engineering

Mechatronics Engineering Programme

MAY 2021

ISTANBUL TECHNICAL UNIVERSITY ★ GRADUATE SCHOOL

IMAGE PROCESSING SOFTWARE TOOLS DEVELOPMENT FOR SHOULDER ARTHROPLASTY

Ph.D. THESIS

Majid MOHAMMAD SADEGHI
(518132013)

Department of Mechatronics Engineering

Mechatronics Engineering Programme

Thesis Advisor: Prof. Dr. Şeniz ERTUĞRUL
Co-advisor: Prof. Dr. Emin Faruk KEÇECİ

MAY 2021

İSTANBUL TEKNİK ÜNİVERSİTESİ ★ LİSANSÜSTÜ EĞİTİM ENSTİTÜSÜ

OMUZ ARTROPLASTİ İÇİN GÖRÜNTÜ İŞLEME YAZILIMI GELİŞTİRME ARAÇLARI

DOKTORA TEZİ

Majid MOHAMMAD SADEGHI
(518132013)

Mekatronik Mühendisliği Anabilim Dalı

Mekatronik Mühendisliği Programı

Tez Danışmanı: Prof. Dr. Şeniz ERTUĞRUL
Eş Danışman: Prof. Dr. Emin Faruk KEÇECİ

MAYIS 2021

Majid MOHAMMAD SADEGHI, a Ph.D. student of ITU Graduate School student ID 518132013, successfully defended the thesis entitled "IMAGE PROCESSING SOFTWARE TOOLS DEVELOPMENT FOR SHOULDER ARTHROPLASTY", which he/she prepared after fulfilling the requirements specified in the associated legislations, before the jury whose signatures are below.

Thesis Advisor :	**Prof. Dr. Şeniz ERTUĞRUL** Istanbul Technical University	.....
Co-advisor :	**Prof. Dr. Emin Faruk KEÇECİ** Abdullah Gül University	.....
Jury Members :	**Prof. Dr. Ayşe ARALAŞMAK** Istinye University	.....
	Prof. Dr. İsmail Kerem BİLSEL Bezmialem Vakif University	.....
	Prof. Dr. Erdinç ALTUĞ Istanbul Technical University	.....
	Assoc. Prof. Dr. Fatih YILDIZ Bezmialem Vakif University	.....
	Assoc. Prof. Dr. Ali Fuat ERGENÇ Istanbul Technical University	.....

Date of Submission : **14 April 2021**
Date of Defense : **21 May 2021**

To my beloved wife and my parents,

FOREWORD

The work carried out in this thesis has been very important to me since it opened to me a new multidisciplinary field of study which enabled me to experience the application of engineering techniques in medicine. This let me use my knowledge to provide a service to society no matter how small. I hope that in the future I will be able to learn more and apply more of my engineering knowledge to the medical field to serve the human kind.

It is a pleasure for me to thank all the individuals that helped me during my Ph.D. studies and I have been exceptionally lucky to receive not only scientific but also emotional and personal support from them.

I want to thank deeply my supervisors Prof. Dr. Seniz ERTUGRUL and Prof. Dr. Emin Faruk KECECI for their guidance and support during my Ph.D. studies.

I want to thank Prof. Dr. Seniz ERTUGRUL for her attentive and generous support during the years of PhD study. She has very patiently helped me during different steps and made this study possible.

I want to thank Prof. Dr. KECECI for his kind and generous supervision and companionship in all aspects of my life. He has always supported me and helped me grow both as an individual and academically. I am definitely indebted to him and hope I can repay him one day by supporting other people as he always does.

I want to thank all the jury members, Prof. Dr. Ayse ARALASMAK, Associate Prof. Dr. Erdinc ALTUG, and Associate Prof. Dr. Fatih YILDIZ for their support and suggestions guided and improved the thesis work. Each has affected my graduate education uniquely and I am thankful for it.

I am sincerely thankful for the support of Prof. Dr. ARALASMAK and the Bezmialem University Hospital radiology department for that made the experiments of this work possible. Prof. Dr. Aralasmak always provided me with guidance for radiology expertise required in the thesis and she kindly helped me when I personally needed medical treatments.

I want to thank Associate Prof. Dr. Erdinc ALTUG for his help and comments on the thesis work, and points and corrections he made to the study.

I am thankful to Associate Prof. Dr. Fatih YILDIZ for his help and his resourceful ideas in the different stages of the thesis study.

I want to express my deepest gratitude to Prof. Dr. Kerem BILSEL who has always helped me with the graduate study work and in my personal life. He has supported this study in many different ways, providing me the chance to attend different surgeries, conferences, gain technical experience in medical fields, and expand my network. I want to thank him for the greatly important personal supports that he has given me in my personal life.

I would like to extend my appreciation to Assistant Prof. Dr. Mehmet KAPICIOGLU and Dr. Okan TEZGEL for their invaluable help.

Assistant Prof. Dr. Mehmet KAPICIOGLU has helped me in designing the analysis of the study, performing the experiments, and evaluating the results and I am deeply thankful for his great help.

Dr. Okan TEZGEL has helped me a lot in performing the experiments, capturing the CT scan images, and we had several very useful discussion sessions on the analysis of the results of the study. I want to thank him sincerely for his support.

I want to thank the TUBITAK BIDEB 2215 program that supported me for some periods of the study.

Finally, I want to thank all my family and friends who assisted and supported me along this path for which without their patience and support this work would have not been possible.

May 2021 Majid MOHAMMAD SADEGHI

TABLE OF CONTENTS

Page

ABBREVIATIONS

2D : Two Dimensional
3D : Three Dimensional
ABS : Acrylonitrile Butadiene Styrene
ANOVA : Analysis of variance
AR : Augmented Reality
CAM : Computer Aided Manufacturing
CGAL : Computational Geometry Algorithms Library
CNC : Computer Numerical Control
CT : Computed Tomography
DICOM : Digital Imaging and Communication in Medicine
EBM : Electron-Beam Manufacturing
FDM : Fused Deposition Modeling
GUI : Graphical User Interface
GDCM : Grassroots DICOM
IDE : Integrated Development Environment
ITK : Insight Segmentation and Registration Toolkit
LOM : Laminated Object Manufacturing
MRI : Magnetic Resonance Imaging
OFF : Object File Format
PET : Polyethylene Terephthalate
PSI : Patient-specific Instrumentation
PLA : Polylactic Acid
RSA : Reverse Shoulder Arthroplasty
SGC : Solid Ground Curing
SLA : Stereolithography
SLS : Selective Laser Sintering
STL : Stereo Lithography
3D : Three Dimensional
UID : Instance Unique Identifier
VTK : Visualization Toolkit

LIST OF TABLES

Page

LIST OF FIGURES

Page

IMAGE PROCESSING SOFTWARE TOOLS DEVELOPMENT FOR SHOULDER ARTHROPLASTY

SUMMARY

Reverse shoulder arthroplasty is an operation performed on shoulder joints with diseases such as osteoarthritis and rheumatoid arthritis, complex fractures of the proximal humerus, and osteonecrosis of the humeral head. This operation can face problems and create risky conditions for the patient, which might end in revision operations.

In this work, methods are investigated to reduce one of the main reasons for the problems faced in reverse shoulder arthroplasty. This main reason is the wrong positioning of the K-wire which itself results in the wrong positioning of the implant baseplate. The wrong positioning can reduce the range of motion of the shoulder or can lead to complete malfunctioning of the joint.

Using pre-operative planning of the surgery, and patient-specific instrumentation, are the solutions evaluated for improvement of the condition and reducing the risk of malpositioning.

Preoperative planning which is deciding the correct choice of the procedure before the operation based on the patient, injury type, facilities available, and surgeon's skills, is an important method in improving implant positioning. Preoperative planning can be performed using two-dimensional images of the patient, but use of three dimensional images and computer preoperative planning software tools can improve planning.

Patient-specific instrumentation which is a modern orthopaedics technique, uses Computed Tomography or Magnetic Resonance Imaging of a specific patient to create customized guides preoperatively. Prostheses or guides that are designed based on the specific anatomy or injury of a patient provide an opportunity to be implemented more precisely and hence can help improve implant positioning and reduce the risk of complications resulting from malpositioning. The PSI guide generation process is performed using software tools that perform preoperative planning on the three-dimensional models of the patient's data.

A new open-source software tool, that provides preoperative planning capability for the surgeon, and also creates a patient-specific guide for K-wire positioning, is developed in this work to test the presented solutions. First, the development of the software, using only open-source platforms, is explained, then using the results of the software an experiment is designed and performed. The experiment evaluated the accuracy of the software results and also compared the results with other existing methods. The experiment contained five different shoulder anatomies and glenoid types. For each type ten different samples were manufactured. Two experienced surgeons experimented on the manufactured bone models and the results were evaluated to differentiate between different anatomies.

The results were evaluated to control the version angle, inclination angle, and the entry point location of the K-wire after the experiment. The evaluation of the results presented that this proposed method has good accuracy for all three parameters. Also, the results showed better outcomes for specific types of anatomies when compared to the freehand method and the conventional guide method.

OMUZ ARTROPLASTİ İÇİN GÖRÜNTÜ İŞLEME YAZILIMI GELİŞTİRME ARAÇLARI

ÖZET

Ters omuz artroplastisi (TAO), ağrı hakim olduğunda, güç veya hareketlilik dahil olmak üzere omuz eklemi işlevselliği bozulduğunda veya kaybolduğunda ve analjezik ve fizyoterapi gibi konservatif tedaviler etkili olmadığında yapılan bir omuz protezi implantasyonudur.

TOA'da, skapula kemiğinin (Kürek kemiği) hem humerus başı hem de glenoid bölümleri implantlarla değiştirilir ancak eklemin anatomisi, glenoide takılan protezin top şeklinde ve humerus kemiğine takılan protezin içbükey bir şekle sahip olacağı şekilde tersine çevrilir.

Ters omuz artroplastisi genellikle başarılıdır, ancak farklı komplikasyonlar ortaya çıkabilir. TOA'daki en yaygın komplikasyonlar instabilite, enfeksiyon ve glenoid gevşemedir. TOA'daki glenohumeral instabilite, eklem protez bileşenlerinin yanlış konumlandırılmasından kaynaklanabilir. Bileşenin mesafe veya açı açısından yanlış yerleştirilmesi instabiliteye neden olabilir. Glenoid implantın doğru yerleştirilmesi, protez dayanıklılığı ve daha iyi omuz fonksiyonu için çok önemlidir fakat, İşlem geleneksel yöntem kullanılarak yapıldığında, daha önce gerçekleştirilen operasyondan sonra kürek kemiğinin değişken anatomisi, eklem kontraktürleri, glenoiddeki kemik kaybı ve güvenilir anatomik işaretlerin olmaması nedeniyle bileşen yerleştirme zor olabilir.

Operasyon öncesi planlama ve hastaya özel kılavuzların kullanımı implant konumlandırmanın iyileştirilmesine yardımcı olabilir ve sonuç olarak yanlış konumlandırmadan kaynaklanan komplikasyon riskini azaltmak için uygun bir çözüm sunabilir. PSI (Hastaya Özel Enstrümantasyon), hastanın anatomisinin gereksinimlerini karşılayan özelleştirilmiş kılavuzlar oluşturmak için belirli bir hastanın Bilgisayarlı Tomografi veya Manyetik Rezonans Görüntülemesini kullanan bir yöntemdir. PSI kılavuz oluşturma süreci, hastanın kemiklerinin üç boyutlu modelleri üzerinde operasyon öncesi planlama yoluyla gerçekleştirilir. Operasyon öncesi planlama, hastayı ve hasar koşullarını değerlendirerek ve cerrahın kullanabileceği imkanları, donanımı ve becerileri göz önünde bulundurarak doğru prosedür ve implant tipi seçimine karar vermektir.

Yazılımın operasyon öncesi planlamada çok önemli yardımı olabilir. Bir hastanın anatomisinin ve özel durumunun üç boyutlu bir modelini görüntülemek, bir cerrahın farklı tedavi çözümlerini belirlemesine yardımcı olabilir. Cerrahın implantı hastanın kemiklerine sanal bir alanda yerleştirme yeteneği, glenoid versiyonun ve eğimin optimal düzeltmesine karar vermede yardımcı olabilir. Ayrıca yazılım PSI kılavuzu oluşturma sürecinin gerekli bir parçasıdır. Bu çalışma, ters omuz artroplastisinde yanlış konumlandırmanın zorluklarının üstesinden gelebilecek bir yazılım aracı oluşturmuştur ve bu tezde, ters omuz artroplastisi için bir PSI, ameliyat

öncesi planlama ve kılavuz tasarım yazılım aracı geliştirme aşamaları ve süreçleri açıklanmıştır.

Böyle bir yazılım aracı geliştirmek için öncelikle farklı tıbbi durumlar araştırıldı ve ardından Bilgisayar Tomography (BT) tarama görüntüleri olarak girdi verilerinin türü ve özellikleri incelendi. Ardından, son yazılıma ulaşmak için giriş verileri üzerinde yapılacak işlemler tasarlandı ve operasyon öncesi planlamanın genel süreci planlandı. Genel süreçler kullanılarak sürecin her bir adımı tasarlandı ve geliştirildi. Her adım için gerekli algoritmalar ve yazılım araçları bulundu, geliştirildi ve entegre edildi. Girilen verileri yakalamak, okumak, yazılım ortamına aktarmak, verileri sıralamak ve kaydetmek için farklı protokoller ve standartlar kullanıldı. Diğer adımlarda kullanılacak en iyi veri yakalama yöntemini sağlayan yazılım için belirli bir BT tarama protokolü seçildi. DICOM standardı, GDCM ve VTK kütüphaneleri daha sonra yakalanan verileri işlemek için kullanıldı. DICOM standardının uluslararası kabul görmüş alanları ve ayrıntıları sayesinde veri işleme çok verimli hale getirildi, GDCM ve VTK kütüphanelerinin kullanılması ile verilere erişimin sorunsuz olması sağlandı. Yakalanan ve sıralanan verilerin ön işleme tabi tutulması için kontrast artırma ve gürültü giderme işlemleri gerçekleştirildi. Verilerdeki önemli bilgileri koruyabilen özel gürültü giderme algoritmaları seçildi ve bunların ITK kütüphanesinde uygulanması ile süreç çok güvenilir hale getirildi. Tüm dokulardan kemiklerin tespiti ve ardından kürek kemiği ve özelliklerinin tespiti için yeni algoritmalar ve yöntemler geliştirildi ve VTK kütüphanesi kullanıldı. Kemikleri diğer dokulardan ayırabilmek amacıyla, her hastanın otomatik eşik tespiti için özel olarak seçilmiş BT tarama protokolü ve hasta verilerini kullanmak üzere yeni algoritma geliştirildi. Diğer kemikler arasından kürek kemiğini tespit etmek için, omuz bölgesindeki kemiklerin geometrik özelliklerinin bir kemik ayırma yöntemi oluşturduğu kabul edildi. Kürek kemiğinin özelliklerini saptamak için birçok farklı geometrik özellik, kürek kemiğinin ve glenoid yüzeyinin genel şekli, nokta ve yüzey algılama algoritmalarının bir kombinasyonu kullanıldı. Algoritmaların bazı bölümlerinde VTK kütüphanesini kullanıldı ve bazı bölümler kütüphanelerin mevcut sorunun belirli gereksinimlerini karşılamadığı için yalnızca C ++ dili kullanılarak geliştirildi. Yazılımın GUI (Grafiksel Kullanıcı Arayüzü) tasarımı ve yazılım destekli operasyon öncesi planlama birlikte gerçekleştirildi. GUI bölümlerinin düzeni ve mevcut özellikler, operasyon öncesi planlama için işlevsellikleri göz önünde bulundurularak tasarlandı. GUI, işleme ve ara yüz tasarımı için VTK ve Qt kütüphaneleri kullanıldı. Operasyon öncesi planlama süreci hem yazılımın teknik yönleri hem de yazılımın kullanıcısı olarak cerrahlardan gelen geri bildirimler dikkate alınarak tasarlandı. Kılavuzu tasarlamak için VTK, CGAL ve OpenMesh kütüphaneleri kullanıldı. Kılavuzun algoritmaları ve geometrik şekli, işlemin her belirli hasta için tam otomatik olabileceği ve kılavuzun glenoid üzerinde uygun oturma ve delme işlemi için iyi mekanik dayanıma sahip olacağı şekilde tasarlandı. Bu çalışmada geliştirilen yöntemler ve algoritmalar, yazılımın her bölümündeki görevleri çözmek için optimize edilmek üzere tasarlandı. Kullanılan kütüphanelerin tümü, diğer geliştiriciler tarafından erişilebilen iyi kurulmuş ve iyi bilinen açık kaynaklı kütüphanelerdir. Tüm bu algoritmalar ve kütüphaneler, her tıbbi vaka için hastaya özel bir kılavuz oluşturma imkânı sağlar. Bu durumlar daha sonra geliştirilen yazılımı test etmek için kullanılabilir.

Yazılımı farklı yönlerden test etmek için bir deney tasarlandı. İlk olarak, farklı hastalar üzerinde operasyon öncesi planlama yapmak için yazılım yeteneği kontrol edildi ve tasarlanan kılavuzların kalitesini gözlemlendi. İkinci olarak, farklı glenoid tipleri

için bu yazılım tarafından operasyon öncesi planlama yapıldığında gerçekleştirilen işlemlerin sonuçlarının doğruluğu kontrol edildi. Bu hedeflere ulaşmak için deneyde, beş farklı kürek kemiği tipinin bilgisayarlı tomografi taramalarını kullanıldı. Çalışma gruplarını oluşturmak için Walch sınıflandırması kullanıldı. Walch sınıflandırmasına göre bir kürek kemiğinin her biri tip A2, B2, C, D idi ve bir kürek kemiği sağlam veya artritik olmayan bir glenoide sahipti. Gerçekleştirilecek deney için, kürek kemiği modellerinin 3 boyutlu hızlı yazıcı ile modellenmesi sağlandı. Toplam 150 tam boyutlu fiziksel kürek kemiği modeli ve 15 kılavuz modeli üretildi. Üretilen kemik modelleri etiketlendi ve kodlandı. Her bir kürek kemiği tipi grubu için deney üç farklı yöntem kullanılarak gerçekleştirildi ve her yöntem iki farklı cerrah tarafından beş kez tekrarlandı.

Deneyin sonuçlarını gözlemlemek için, modellerin ve kılavuz pinlerin operasyon sonrası BT taramaları, yazılımla kullanılacak ilk görüntüleri yakalamak için kullanılan aynı BT tarama protokolü kullanılarak elde edildi. Daha sonra, bu BT görüntüleri, kemiğin içinde yer alan kılavuz pim ile kemiklerin 3D modellerini oluşturmak için kullanıldı. Her numunenin 3D modelleri, birbirleriyle tam olarak eşleşecek şekilde 3D alana kaydedildi. Daha sonra Friedman ve Maurer yöntemleri kullanılarak, 3 boyutlu modellerin versiyonu ve eğimi dijital olarak ölçüldü. Kılavuz pim girişinin glenoid yüzeye pozisyonu da planlanan giriş noktasına göre ölçüldü. Versiyonun ortalama değeri ve standart sapması, eğim ve giriş noktası konumları, her yöntemle çalıştırılan her numune için ölçüldü.

Bu çalışmanın hipotezlerinden biri, diğer PSI olmayan omuz artroplasti operasyonlarına kıyasla operasyon öncesi planlama yeteneklerini ve PSI kılavuzlarını yüksek doğrulukla kolaylaştırabilen açık kaynaklı bir yazılım platformunun geliştirilebileceğidir. PSI yönteminin geleneksel yöntemlerle karşılaştırılması için sonuçların değerlendirildiği durumlarda, PSI yönteminin hata değerleri diğer yöntemlerden daha iyi ortalama ve standart sapma göstermiştir, PSI yönteminin operasyon sonrası değerleri, planlanan değerler ve hastaya özel kılavuz, planlanan değerlerle birbirine iyi derecede yakındır.

Bu çalışmanın bir başka hipotezi, operasyon öncesi planlama yazılımı kullanılarak tasarlanan PSI'lerin, özellikle glenoid kemik deformesi vakalarında, standart kılavuzlu ve serbest el enstrümantasyon yöntemlerinden daha iyi kılavuz pim konumlandırma sağlayabileceğidir. Glenoid gruplarının çoğu için farklı tipteki glenoidlerin hata değerlerinin PSI için daha iyi ortalama ve standart sapma değerleri gösterdiği görülmüştür. Bu çalışmanın sonuçları, PSI'nın kılavuz pim konumlandırma doğruluğunu göstermiştir ve artritik olmayan glenoid tipi ve kusurlu glenoid tipleri C, B2 ve A2 için, PSI'nın diğer yöntemlere göre daha doğru olduğunu göstermiştir, fakat bu sonuçlar istatiksel anlamda artritik olmayan glenoid tipi ve C glenoid tipi için anlamlıdır.

Genel olarak, çalışma sonuçları, kanıtlamaya ve ulaşmaya çalıştığı ilk amaçları ve hipotezleri desteklemektedir ve yalnızca açık kaynaklı kütüphaneler kullanılarak geliştirilen araç, daha fazla araştırma için bir kılavuz olabilir.

1. INTRODUCTION

1.1 Purpose of the Thesis

Reverse shoulder arthroplasty (RSA) faces complications and the most common complication is component loosening. Incorrect positioning is one of the main factors for glenoid component loosening in reverse shoulder arthroplasty. The correct component placement in RSA can be difficult due to different anatomical and surgical challenges.

Patient-specific instrumentation (PSI) has shown improvements in the accuracy of surgical operations including component positioning in RSA. PSI needs software tools for performing preoperative planning for shoulder arthroplasty and the design of a proper instrument or guide to help with the correct positioning.

In the existing studies, the improvement in accuracy of operation is not evaluated on different types of glenoids in RSA. There are several commercial PSI systems available that can be used in an operation but the computer techniques and tools used to develop such software packages are not fully presented in academic literature, because of trade secrecy.

This work intends to create a software tool that can overcome the challenges of incorrect positioning in reverse shoulder arthroplasty. This software tool aims to reach this goal by enabling surgeons with preoperative planning for RSA, and designing a new guide for the surgery while implementing merely open-source libraries.

1.2 Problem Definition

Reverse shoulder arthroplasty (RSA) is generally successful, although different complications can occur. The most common complications in RSA are instability, infection, and glenoid loosening [1–3]. Glenohumeral instability in RSA can be caused by malpositioning of the joint prosthesis components. Any misplacement of the

component in distance or angle can cause instability [4–6]. In conventional methods, the identification of anatomical landmarks and accurate positioning of the implant baseplate are difficult to achieve when there are deformities in the glenoid cavity [7]. For instance, the implant inferior version and tilt angle have shown 16 - and 12-degree variations, respectively, in traditional surgery methods [8]. Conventional methods of implantation are not able to restore the retroversion angle in cases with severe glenoid deformity [9, 10]. Correct placement of the glenoid implant, which is one of the main goals of preoperative planning, is crucial for prosthesis durability and better shoulder function [11, 12], however component placement can be challenging because of the variable anatomy of the scapula, joint contractures, bone loss in the glenoid, and lack of reliable anatomic landmarks after the previous operation [13].

Preoperative planning and the use of patient-specific guides can help improve implant positionin [14–17] and as a result could present a proper solution to reduce the risk of complications resulting from malpositioning. PSI uses Computed Tomography (CT) or Magnetic Resonance Imaging (MRI) of a specific patient to create customized guides preoperatively and the PSI guide generation process is performed through preoperative planning on the three-dimensional models of the patient's bones.

Software can be of great help in preoperative planning and creating patient-specific guides. Viewing a three-dimensional (3D) model of the anatomy of a patient and their specific condition can help a surgeon to determine different treatment solutions. The ability of the surgeon to place the implant into the patient's bones in a virtual space can help in deciding the optimal correction of the glenoid version and inclination [18–22]. The use of patient-specific guides for glenoid component placement has increased the reliability and precision of shoulder arthroplasty [13, 17, 23–25]. Furthermore, it should be considered that Guide pin positioning has a direct effect on the initial glenoid component placement.

Consequently, in this thesis, the problem of developing an open source software tool that can reduce the complications of RSA through enabling preoperative planning and PSI guide design is faced, understanding that the development of such software tool opens a door for the development of other software tools for other surgeries.

1.3 Hypothesis

In this study, we try to explain the steps and processes of developing a PSI preoperative planning and guide design software tool for reverse shoulder arthroplasty. By describing the open-source software packages and platforms used and the logic behind the design of the guide system, the authors believe this study can help to facilitate future studies creating PSI systems. Under the hypothesis that PSIs designed using the preoperative planning software would provide better guide pin positioning than standard guided and freehand instrumentation methods, especially in cases of glenoid bone deformity, the accuracy of the developed software and PSI in different glenoid types are evaluated in this thesis. In summary, this work hypothesizes that an open-source software platform can be developed that can facilitate preoperative planning abilities and PSI guide creations with high accuracy compared to other non PSI methods of shoulder arthroplasty operations.

1.4 Thesis Outline

The thesis is organized into seven chapters. Chapter one is the introduction. Chapter two is background and literature review, where information about different aspects of the works done in the thesis is provided and similar works are reviewed. Chapter three explains the steps of the software development and details of the algorithms used. Chapter four describes the experimentation using the results of the software. Chapter five reports the results of the experiment. Chapter six discusses the results and their implications. Chapter seven is the conclusion and future works that can be performed.

2. BACKGROUND AND LITERATURE REVIEW

In this chapter background information related to the topics discussed throughout the thesis is provided. Medical information about the shoulder joint that is required to understand the problem at hand and the solutions proposed is presented. Information about digital image processing including the tools, standards, libraries, and methods used are demonstrated. At the end of this chapter works similar to this thesis study are discussed.

2.1 Anatomy of the Shoulder Joint

The shoulder joint is one of the most complex joints of the body. It consists of three bones, the humerus, which is the upper bone of the arm, the scapula, which is the shoulder blade bone, and the clavicle, which is the collarbone. The clavicle connecting at one end to the chest bone, and the other end to the acromion of the scapula, attach the upper limb and the trunk.

The scapula bone is a flat and triangular shaped bone. The coracoid process of the scapula is a thick curved section that projects from the scapula and is the attachment point of ligaments and muscles. The glenoid cavity of the scapula is the part that articulates with the head of the humerus and forms the ball and socket shaped joint.

The humerus has a head at its top end with a half-spherical shape projecting into the glenoid cavity. The greater and lesser tubercles are the attachment points for the rotator cuff muscles. In Figure 2.1, anatomy of the shoulder joint is presented.

The rotator cuff is a collection of muscles and tendons that enables a wide range of motions for the shoulder. In Figure 2.2 rotator cuff muscles are shown.

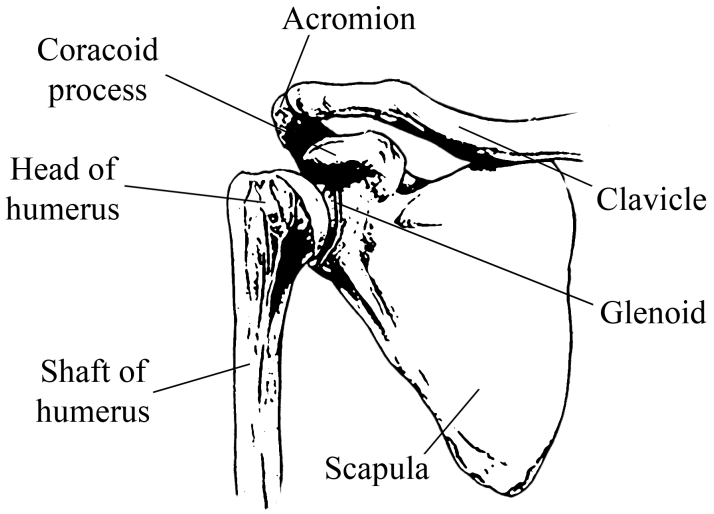

Figure 2.1 : Shoulder Joint Anatomy.

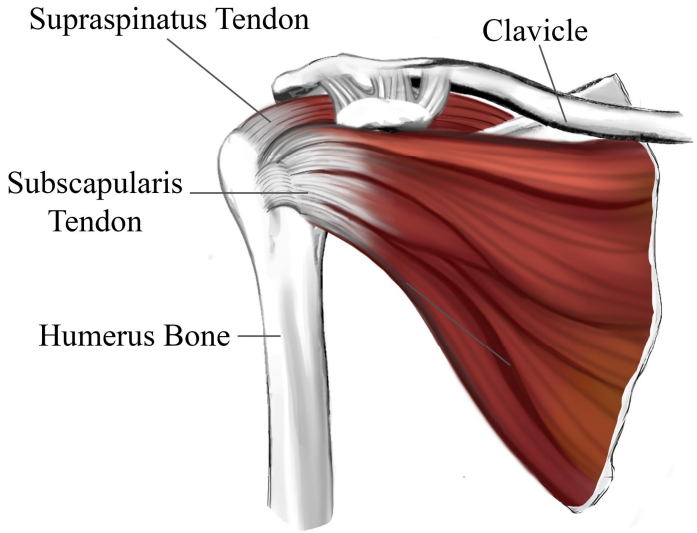

Figure 2.2 : Rotator Cuff Muscles.

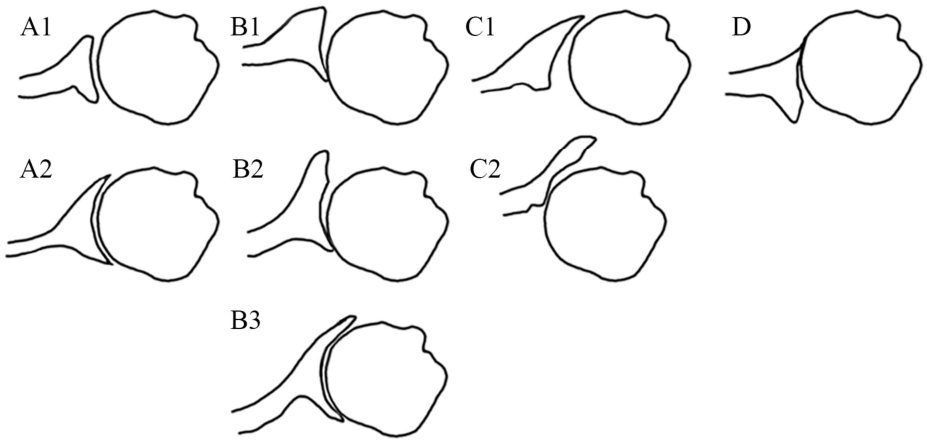

Figure 2.3 : Walch classification of damaged glenoid morphology.

2.1.1 Glenoid morphology classifications

It is necessary to understand and categorize the glenoid deformation before deciding on any treatment for operating the damaged shoulder joint. Knowing the type of deformation can help categorize the outcome of treatment and assist in preoperative planning of the operation. Two different classification methods are wildly used that are described here. The first method is the Walch classification of glenoid morphology [26]. This method has been modified and improved over the years and the most recent method is based on the evaluation of glenoids from 3D CT scan reconstructions.

There are four main categories and a total of eight subcategories in this classification method based on the pathologic glenoid type as shown in Figure 2.3. Type A has concentric wear with no subluxation of the humeral head and the humeral head is centered. A1 type has minor central erosion, while A2 type has major erosion and the humeral head protrudes into the glenoid cavity. Type B has a biconcave glenoid with asymmetric wear and the humeral head is subluxated posteriorly. B1 has posterior joint narrowing (no posterior bone loss), osteophytes, or subchondral sclerosis. B2 has posterior rim erosion or retroverted glenoid. B3 has monoconcave and posterior wear with retroversion bigger than 15° or posterior humeral head subluxation bigger than 70%, or both. Type C1 has a dysplastic glenoid with bigger than 15° retroversion regardless of the erosion. Type C2 has biconcave, posterior bone loss, posterior translation of the humeral head. Type D has glenoid anteversion or anterior humeral head subluxation smaller than 40°.

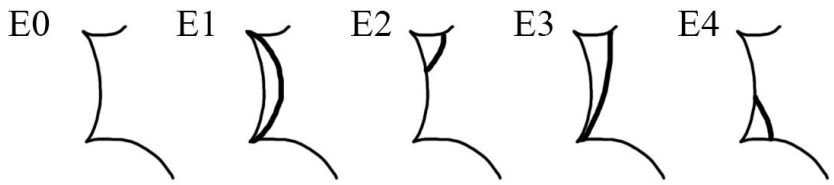

Figure 2.4 : Favard classification of damaged glenoid morphology.

The second classification method is Favard classification [27]. The Favard classification has also improved over time and the latest version has five different categories as shown in Figure 2.4. Type E0 has no glenoid erosion and superior humeral head migration. Type E1 has concentric erosion of the glenoid. Type E2 has erosion of the superior aspect of the glenoid alone. Type E3 has superior erosion extending all the way to the inferior aspect of the glenoid, and type E4 is inferior wear of the glenoid.

2.1.2 Glenoid's version and inclination angles

The Friedman method is a well-established one for measuring the glenoid version angle [28]. In this method, a CT scan of the scapula section, located in the mid glenoid level, in the axial plane is used for the measurement. As shown in Figure 2.5. To find the version angle, first, a line that connects the anterior and posterior rim of the glenoid is drawn, named glenoid line. Next, the center of the glenoid is connected to the root of the scapular spine, which defines the scapular axis. Then the version angle is the angle between the line that is perpendicular to the scapular axis and the glenoid line.

To measure the inclination angle the Maurer method is used [29]. In this method on the oblique coronal plane of the scapula in a section that passes through the glenoid center, the glenoid fossa line is drawn. The glenoid fossa line is the line that connects the uppermost and lowermost points of the glenoid rim. Next, the line of the floor of the supraspinatus fossa is drawn. The inclination angle is defined as the angle between the glenoid fossa line and the line of the floor of the supraspinatus fossa as shown in Figure 2.6.

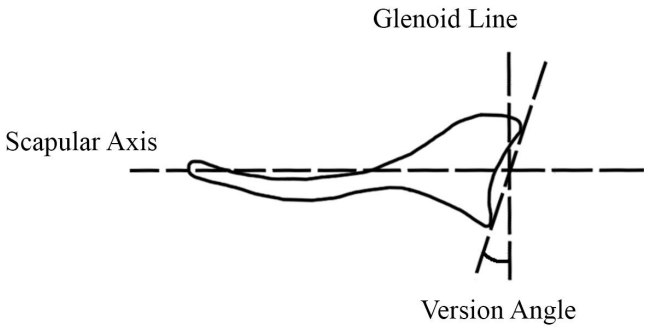

Figure 2.5 : Definition of Version Angle by Friedman.

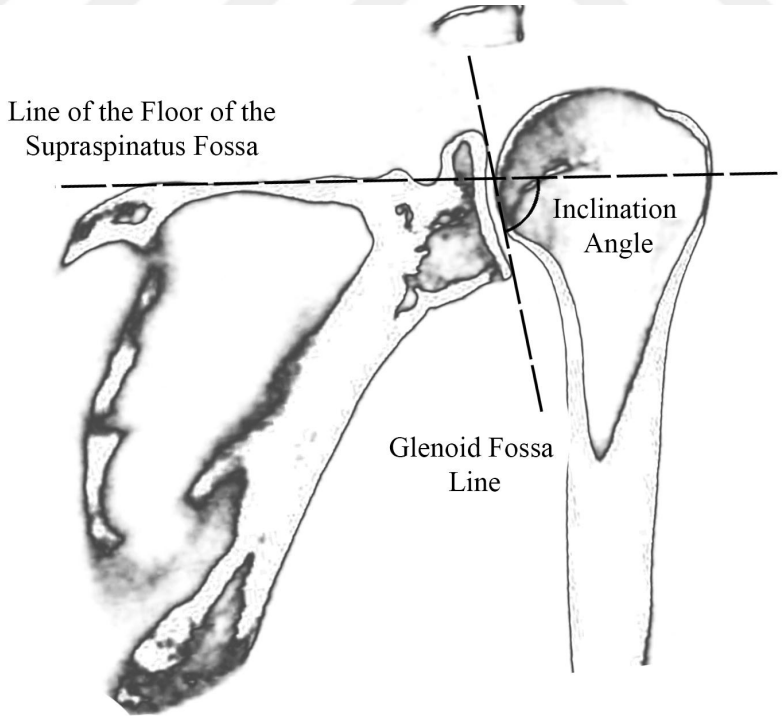

Figure 2.6 : Definition of Inclination Angle by Maurer.

Figure 2.7 : Rheumatoid Arthritis Condition, an Example reason for Shoulder Arthroplasty.

2.2 Shoulder Arthroplasty

Shoulder arthroplasty is performed when pain prevails or shoulder joint functionality including strength or mobility is deteriorated or lost and conservative treatments like Analgesics and physiotherapy are not effective [1]. Common issues, which can result in shoulder arthroplasty, include osteoarthritis, rheumatoid arthritis (Figure 2.7), complex fractures of the proximal humerus, and osteonecrosis of the humeral head. Shoulder arthroplasty is performed also as revisions of failed prosthesis operations [1].

Osteoarthritis is caused by mechanical wear and tear in the joint, for instance when the half-spherical shaped head of the humerus or the glenoid cavity is worn out or damaged. Rheumatoid arthritis is an autoimmune system disease when the damage to the joint happens by the body's own immune system.

Shoulder prosthesis implantation history starts in 1893 when Pean, a French surgeon, performed the first shoulder joint replacement [2]. Later in 1970, shoulder arthroplasty began to get more attention when Charles Neer published an article reporting a 90% success rate in 43 patients with shoulder arthroplasty [3]. In the 1980s, modular prostheses with two components and in different sizes were introduced which lead to more successful operations [4].

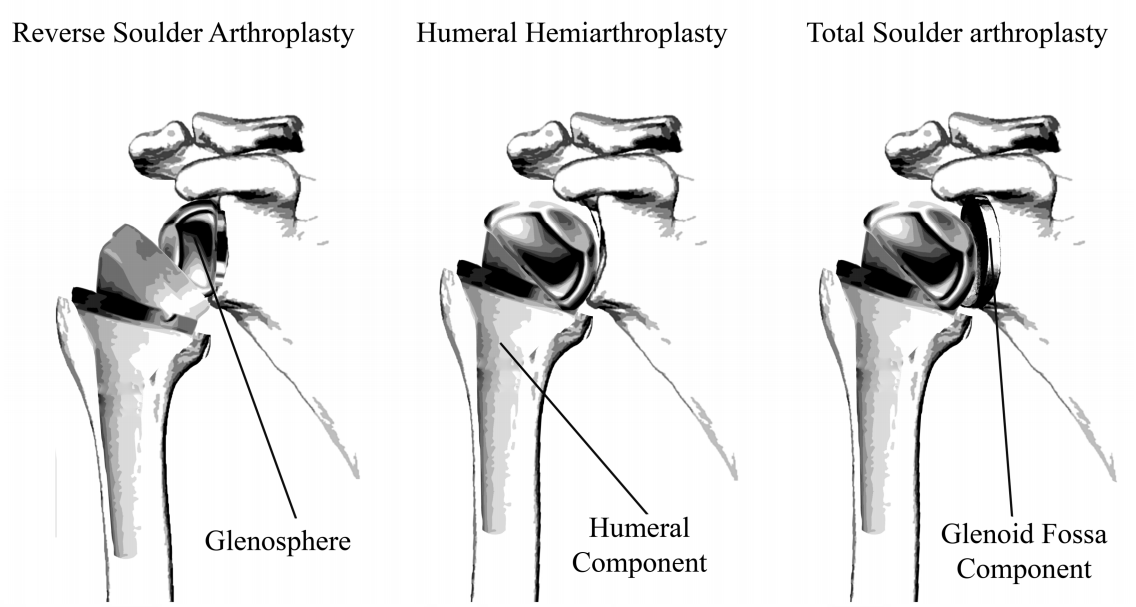

Figure 2.8 : Different Types of Shoulder Arthroplasty.

2.2.1 Shoulder arthroplasty types

Shoulder arthroplasty operations include humeral hemiarthroplasty, Total shoulder arthroplasty, and reverse shoulder arthroplasty as shown in Figure 2.8. [1]. Humeral hemiarthroplasty is replacing the humeral head with an artificial implant in the joint. Total shoulder arthroplasty is performed by replacing both the humeral head and glenoid sections of scapula bone. Major indications for total shoulder arthroplasty are primary and secondary osteoarthritis, as well as early rheumatoid arthritis [1].

In reverse shoulder arthroplasty, the anatomy of the joint is reversed in a way that prosthesis attached to the glenoid has a ball shape and the prosthesis attached to the humeral bone has a concave shape.

Reverse shoulder arthroplasty has been proved as a successful method for treatment in cases with the rotator cuff deficiency [5, 6]. Severe damage or tears to rotator cuff and revision surgery are among the reasons to perform reverse shoulder arthroplasty (Figure 2.9) [1].

In reverse shoulder arthroplasty, medialization and distalisation in the shoulder joint, meaning that the center of rotation is moved downwards and closer to the body, prevents the shoulder to move upward out of its center and also increases the force moment that the deltoid muscle can create, and as a result, lifting of the arm is improved as shown in Figure 2.10 [30].

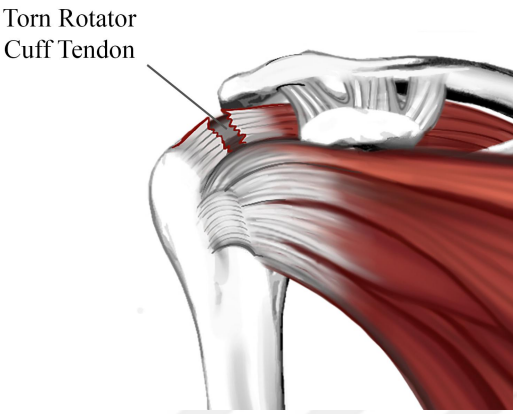

Figure 2.9 : Rotator Cuff Tear, as a Symptom Leading to Reverse Shoulder Arthroplasty.

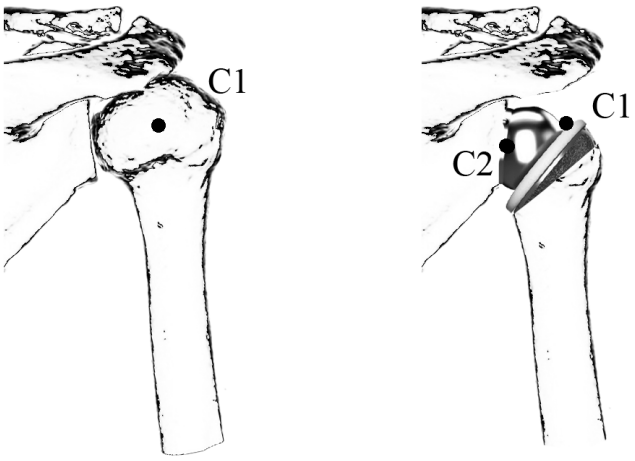

Figure 2.10 : C1 is the anatomic center of rotation of joint and C2 is the center of rotation after RSA. It is observed that C2 is distalized and medialized.

Figure 2.11 : General Type of Implant Used for RSA (image by DELTA CTA™ Reverse Shoulder Prosthesis, Deputy).

The general implant type used for reverse shoulder arthroplasty is shown in Figure 2.11.

2.2.2 General operation procedure

To perform the operation, first the surgeon enters the shoulder joint by making an incision into the joint capsule. This allows the surgeon to access the joint. At this point, the surgeon can prepare the bones for attaching the prosthesis parts. The preparation of the humeral bone is done by removing the ball portion of the humeral head with a bone saw. Then a rasp is used to prepare inside of the humeral bone to anchor the stem of the humeral component. Figure 2.12 shows humeral components of the implants inserted.

For the preparation of the glenoid side, a guide pin is inserted into the glenoid cavity to be used as the reference for the next operations of the surgery. Using the guide pin (Kirschner wire) inserted, the arthritic glenoid surface is prepared by reaming the surface and cleaning any remaining cartilage. With the reaming, the surface of the glenoid is flattened and a proper resting area for the base plate is provided.

Figure 2.12 : Humeral Components Inserted (image by DELTA CTA™ Reverse Shoulder Prosthesis, Deputy).

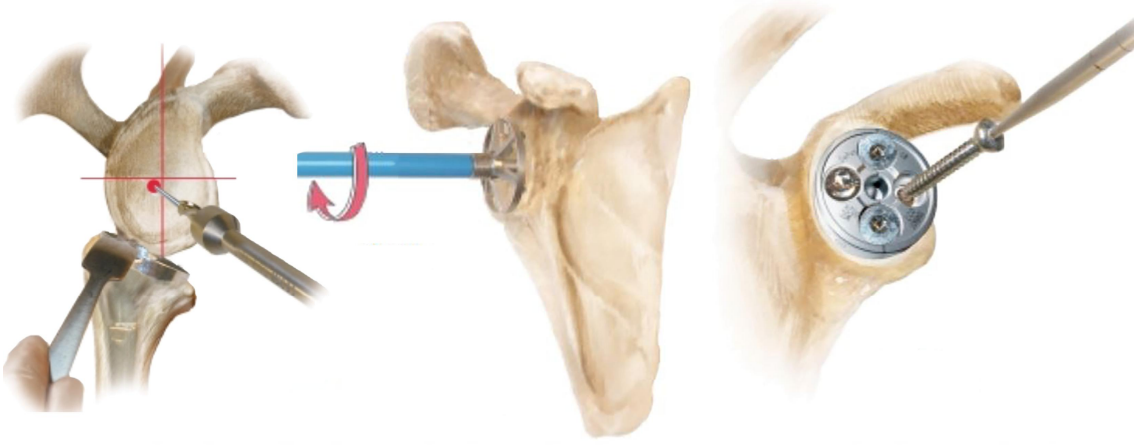

Figure 2.13 : The Preparation of Glenoid Surface for Implantation (image by DELTA CTA™ Reverse Shoulder Prosthesis, Deputy).

At this stage, the central peg drilling is performed using the guide pin for baseplate fixation. Next, the base plate is fixed on the reamed glenoid surface using the central part and side screws as shown in Figure 2.13.

Then the glenoid sphere is attached to the base plate. The surgeon controls the proper functioning of the shoulder after the joint is anchored and then stitches the joint capsule, and closes the incision as can be observed in Figure 2.14.

2.3 Preoperative Planning In Shoulder Arthroplasty

Preoperative planning is deciding the correct choice of the procedure and implant type, by evaluating the patient and injury conditions and considering facilities, equipment, and skills available to the surgeon.

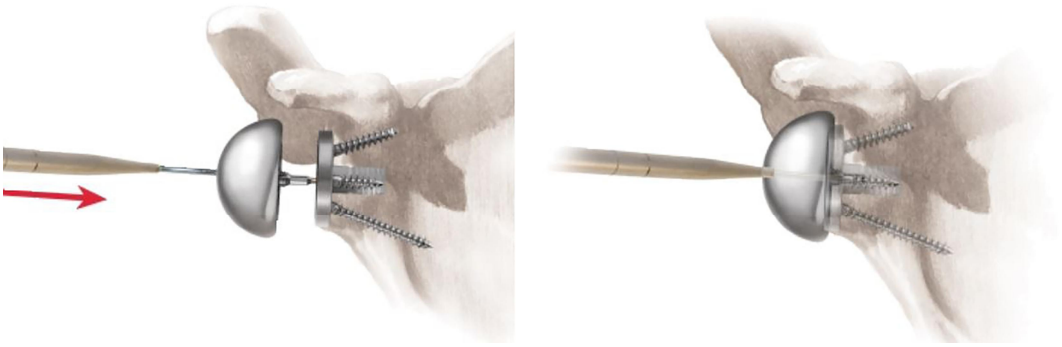

Figure 2.14 : The Attachment of Glenoid Sphere to the Baseplate (image by DELTA CTA™ Reverse Shoulder Prosthesis, Deputy).

Standard preoperative planning for reverse shoulder arthroplasty starts with a radiographic analysis of the anatomy of the shoulder joint. Two-dimensional CT scan images from different views can be used for this step. If rotator cuff condition is not understood from the physical examinations then magnetic resonance imaging of the joint can be performed. Also if the case has a large glenoid deformity, a three dimensional CT scan provides better information on the anatomy of the glenoid. Using this information the surgeon decides about the operation details beforehand including the best orientation of the guide pin in the glenoid cavity, and he uses the same information intraoperatively.

Computer preoperative planning uses software tools for creating an interactive three-dimensional environment in which the surgeon can better observe the anatomy of the shoulder. Using this tool, improved planning can be achieved.

2.4 Patient Specific Instrumentation

Patient specific instrumentation helps the surgeon by creating prostheses or guides that are designed based on the specific anatomy or injury of a patient. In reverse shoulder arthroplasty a couple of guides can be used during the operation. In this work, a patient specific guide is considered to be developed for placement of the K-wire pin to the glenoid cavity. This PSI guide provides an opportunity to increase the precision in the implementation of the preoperative planning performed for the patient.

PSI takes advantage of three dimensional image processing and computer planning to design a particular guide model to be used intraoperatively by the surgeon. PSI guides have several landmarks that are used for proper positioning on the bones based on the

anatomy of the patient. After the PSI models are designed, they are manufactured and physical models are used during the operation.

2.5 Digital Image Processing in Medical Field

Digital image processing is applied in various medical fields aiming to help human health improvement. It is a multidisciplinary field where computer science, mathematics, and medicine are bonded together so that meaningful solutions can be created for health related issues.

Image processing techniques are used in a wide range of medical applications, including orthopaedics. Arthroplasty operations in different parts of the body benefit from image processing tools. Shoulder arthroplasty as a prostheses operation also can use the advantages image processing can provide. Major areas of image processing, libraries developed, and methods in image processing that are used in this work are explained in the following sections.

2.5.1 Major areas of image processing

Digital image processing can be categorized into five different groups all of which are used for medical applications. These groups consist of image acquisition, image enhancement, image analysis, visualization, and data management [31].

Image acquisition varies widely based on the input signal used for imaging. For example, CT scan, and MRI imaging systems have different acquisition and capturing methods.

Computer Tomography (CT) imaging uses X-rays measurements passing through body parts. The attenuation in the intensity of X-ray beams passing through a substance depends on the density and thickness of the substance. Hence higher density materials like bones that absorb more X-ray, appear in a lighter color in CT images, while lower density materials like fat and muscles appear darker.

Magnetic resonance imaging (MRI) uses a magnetic field and radio waves for image acquisition. Hydrogen atoms exist abundantly in the body, especially in water and fat. A magnetic field is used for the polarization of the hydrogen atomic nuclei existing in the body. Then a burst of radio waves is sent to the area being imaged, which

is absorbed by the hydrogen atomic nuclei. After the sent radio wave is stopped, the radio frequency waves induced from the spin polarization are absorbed by the receivers close to the body. Using this technique, tissues of the body with different water and fat amounts can be detected.

Image enhancement processes are performed on the images to reduce noise and increase the quality of the images. These operations are low-level analyses of the data in which a knowledge of the content of the image does not have to be known. Image enhancement results can be used directly by a human observer or can be used as a pre-processing step for other computer processes. Processes like, image transformation, registration, noise reduction, and other filtering operations are among image enhancement processes.

Image analysis processes like feature extraction, segmentation, or classification are higher-level processes that extract some level of information from the image. In medical applications, this type of process creates the chance for differentiating and separating tissues or organs from each other, and extracting meaningful features that will be used for diagnosis or treatment purposes.

Visualization is the process of presenting the raw or analyzed image data through a medium to be observable for the human user. Visualization techniques specifically are important when volumetric data is to be visualized and the human user must access the information in 3D space. Rendering, displaying, and manipulating of the computer models are among the processes in this section.

Data management processes include compression, storage or retrieval of data, and communication of the data between different mediums. Compression techniques are increasingly getting important due to the increased number of images taken and the size of images. Lossless compression methods are preferred especially in the medical field because of the importance of the details presented in the images for diagnostic purposes. Better compression techniques facilitate storage, transmission, and access to the image data.

2.5.2 DICOM storage and communication format

Different commercial equipment from a variety of manufacturers is used to capture medical images. Digital Imaging and Communication in Medicine (DICOM) standard has been created to handle this situation. It is a non-proprietary protocol which helps with safe data exchange in medical fields [32]. Using DICOM standard enables a shared format between all devices so that regardless of the type of the instrument used for imaging, or the manufacturer of instrument, images can be accessed. DICOM standard provides data structures, including more types of data besides the image data. The main components of the data structures are Information Object Definitions (IODs), which can include a patient's data, medical device's data, medical institutions data, reports associated with the image, and much other optional information [33]. This data are stored in a header section and are of great importance for stable and accurate reading and evaluation of images. DICOM standard images can be accessed and viewed by dedicated DICOM viewers and other third-party viewers, which have been available in recent years.

2.5.3 Libraries for image analysis

In this section image processing libraries used in the thesis are described. These libraries are all open source and include capacities for data management, modelling and visualization, user interface design, and three dimensional Boolean operations. Knowing these libraries and their capabilities are required to understand the works done in this study.

2.5.3.1 Grassroots DICOM (GDCM)

GDCM is a C++ library for handling DICOM standard files. It is designed as an open source library to facilitate access to clinical data directly for researchers across different fields [34]. GDCM includes both a network communication protocol and a file format definition. It is originally written in C++ language but offers wrapping for other languages including Python, C#, Java, PHP, and Perl. It tries to cover all DICOM image formats namely:

• RAW,

• JPEG lossy 8 & 12 bits (ITU-T T.81, ISO/IEC IS 10918-1),

• JPEG lossless 8-16 bits (ITU-T T.81, ISO/IEC IS 10918-1),

• JPEG 2000 reversible & irreversible (ITU-T T.800, ISO/IEC IS 15444-1),

• RLE,

• Deflated (compression at DICOM Dataset level),

• JPEG-LS (ITU-T T.87, ISO/IEC IS 14495-1),

• JPEG 2000 Multi-component reversible & irreversible (ISO/IEC IS 15444-2) (not supported for now),

• MPEG-2 (not supported for now).

GDCM is a cross platform library that can target Win32 and MacOSX systems and compiles with many C++ compilers including gcc, icc, clang, and Visual C++. It has a nightly dashboard where the whole library is controlled.

An important feature of this library is that it has bridge classes to VTK and ITK libraries. Classes vtkGDCMImageReader/vtkGDCMImageWriter/vtkGDCMPolyDataReader are to be used to communicate with VTK library and class itk::GDCMImageIO is to be used by ITK software developers.

2.5.3.2 The Visualization Toolkit (VTK)

VTK is an open source library for image processing, modeling, rendering, visualization, and plotting [35]. This library covers a huge variety of algorithms and techniques and contains a great number of classes. The visualization algorithm comprises scalar, vector, tensor, texture, and volumetric methods. Also modeling techniques like implicit modeling, polygon reduction, mesh smoothing, cutting, contouring, and Delaunay triangulation are included in the library.

The main features of VTK are developed in C++ to have the maximum efficiency, and then they are wrapped into different languages to provide maximum usability by researchers with different background knowledge. The Python wrap of the VTK library is especially well developed since python is a very common language.

VTK can use both threaded and distributed memory parallel processing for speed and scalability. It is platform independent and can run on Mac, Linux, Windows, on mobile devices, and on the Web.

The community supporting for VTK is an active distributed one that provides a reliable code. Kitware Inc also provides professional support for VTK.

2.5.3.3 The Insight Toolkit (ITK)

ITK is an open source library that is mainly developed to perform segmentation and registration operations [36]. ITK segmentation process is mostly applied to medical images captured by CT scan or MRI technologies. The algorithms in ITK can be applied to two, three, and arbitrarily more dimensions of data types.

ITK is a cross platform library and uses CMake build environment to handle the generation of projects on different platforms. This library is written in C++ and uses a generic programming method, which makes it very efficient, and debugging of the code can be performed easier at compile time.

ITK is wrapped for Python and many other languages including, Java, CSharp, R, Tcl, and Ruby. ITK is actively developed and maintained by a community of research software engineers from around the world.

2.5.3.4 Qt

Qt is an open-source toolkit that is developed for the creation of user interfaces and cross-platform applications [37]. Apart from the open source licenses, this library is also provided with commercial licenses. Qt can be used with many desktop platforms including Linux, OS X, Windows, VxWorks, QNX, Android, iOS, BlackBerry, and Sailfish OS. It also supports mobile and embedded platforms.

Different compilers like GCC, ICC, and MinGW C++ compilers, the Visual Studio suite, PHP via an extension for PHP5 are supported by Qt.

In addition to being a GUI library, Qt is also a toolkit for cross-platform development in fields like networking, databases, OpenGL, web technologies, sensors, communications protocols (Bluetooth, serial ports, NFC), XML and JSON processing, printing, PDF generation, and many more. Programs that do not include GUI, like command-line programs, and consoles for servers, can be also developed by Qt.

Qt has qmake build system of its own, but can also use CMake to build Qt projects and it also integrates a module named QtQuick that makes it easier and faster to build GUIs with QML language. QML uses Javascript to provide procedural programming capabilities. QML can be used to write all the sections of the program but often it is only used for the GUI section and the other sections are written in C++.

Qt also provides Qt Quick, which includes a declarative scripting language called QML that allows using JavaScript to provide the logic. With Qt Quick, rapid application development for mobile devices became possible, while logic can still be written with native code as well to achieve the best possible performance.

Qt programs can be developed without using any Integrated Development Environment (IDE), but it comes with its own IDE named Qt Creator that can be run on Linux, OS X, and Windows. Qt Creator has many different features that a modern IDE has including intelligent code completion, syntax highlighting, an integrated help system, debugger and profiler integration, and also integration for all major version control systems. For windows users, Qt's Visual Studio Add-in can be used as IDE.

Qt Designer is a module included in Qt that generates code for widget based GUIs and can be used independently or as part of the Qt Creator.

2.5.3.5 The computational geometry algorithms library (CGAL)

CGAL is an open-source library that provides efficient and reliable algorithms for geometrical operations [38]. This library is in C++ but can support Python and Java languages.

Among the algorithms and data structures that are provided by CGAL following can be mentioned; triangulations, Voronoi diagrams, Polygons, Cell Complexes and Polyhedra, arrangements of curves, mesh generation, geometry processing, convex hull algorithms. These algorithms are operated on CGAL geometrical objects that are grouped in CGAL Kernels. Spatial sorting functions and matrix search framework, plus linear and quadratic solvers are available on the geometrical objects.

CGAL library has interfaces to communicate with other libraries like Qt, Geomview, and the Boost Graph Library.

MS Visual C++ 14.5, 15.9, and 16.0 are supported compilers for CGAL. There are required libraries that must be preinstalled for CGAL, namely Boost, GNU Multiple Precision Arithmetic (GMP), and GNU Multiple Precision Floating-Point Reliably (MPFR).

If Vcpkg library manager is used to install CGAL, the required libraries and their proper version are automatically found and installed. Otherwise, They must be installed manually prior to CGAL installation.

Although CGAL is an Open source library, commercial licensing can be purchased for industrial applications.

2.5.3.6 Open Mesh

Open mesh is a library that makes it easy to save and manipulate meshes using a generic and efficient data structure [39]. The library was funded by the German Ministry for Research and Education (BMBF) and is developed at the Computer Graphics Group, RWTH Aachen.

Open mesh is flexible in a way that many different algorithms can be used without needing adaptation between them. Open Mesh is efficient; meaning the amount of memory used is kept as low as possible for different algorithms. The interface of Open mesh code is easy to use as complex structures are wrapped by simple commands.

Some of the features provided by Open mesh are as follows:

• Arbitrary polygonal and pure triangle meshes can be represented

• Explicit representation of vertices, half edges, edges, and faces are provided.

• Fast neighborhood access, especially the one-ring neighborhood is possible.

• The coordinate type can be chosen (dimension and scalar type).

• User-defined elements/functions can be attached to the mesh elements.

• User attributes can be attached and checked.

• Data can be attached at runtime using dynamic properties.

Open mesh library provides sample applications in default like Mesh Smoothing, Mesh Decimation, and Qt integration.

2.5.4 Noise removal

Medical images acquired through a CT scan can suffer from noise corruption and can be captured in a narrow range of grayscale values [40, 41].

Medical images captured by different imaging technologies are each affected by different types of noises. The type of noise prevailing in an image depends on the image collection technology and the type of sensor which is used to capture the data. Among different types of noises that can exist in medical images Gaussian noise [42], Poisson noise [40], and Rician noise [43] are the most prevailing types.

MRI images are mostly corrupted by Rician noise [41] while noises in Computed Tomography images are found to be of Poisson distribution [40]. Noise corrupts medical images in many ways including blurring important details of the image like edges and boundaries of tissue parts, or structural details in an organ. It is important to preserve these features of medical images by reducing the amount of noise presented.

In this work, accurate separation of bones from the other tissues presented in the image is of great importance since the software aims at modeling the patient's joint anatomy for the surgeon and the created model geometrical accuracy must be as high as possible. For this reason, the noise reduction method used in this work must be able to keep the sharp edges between bone boundaries and other tissues in the image, while trying to remove noises in all parts of the image.

2.5.4.1 Bilateral noise removal filter

Bilateral noise removal filter is an edge preserving method which is commonly used in medical applications [44]. The bilateral filter is a non-linear filter and it acts on each pixel of the two-dimensional image by replacing it with an average value of its surrounding pixels. The selection of surrounding pixels to be used in the averaging operation and their corresponding weights in the calculation are of a specific method, which makes the filter an edge preserving filter. In this method, there exist two different criteria for weighting of the surrounding pixels. The first criterion is a spatial kernel with a Gaussian distribution, which assigns higher weights to the pixels closer to the central pixel being proceeded. This part only considers the geometrical distance of

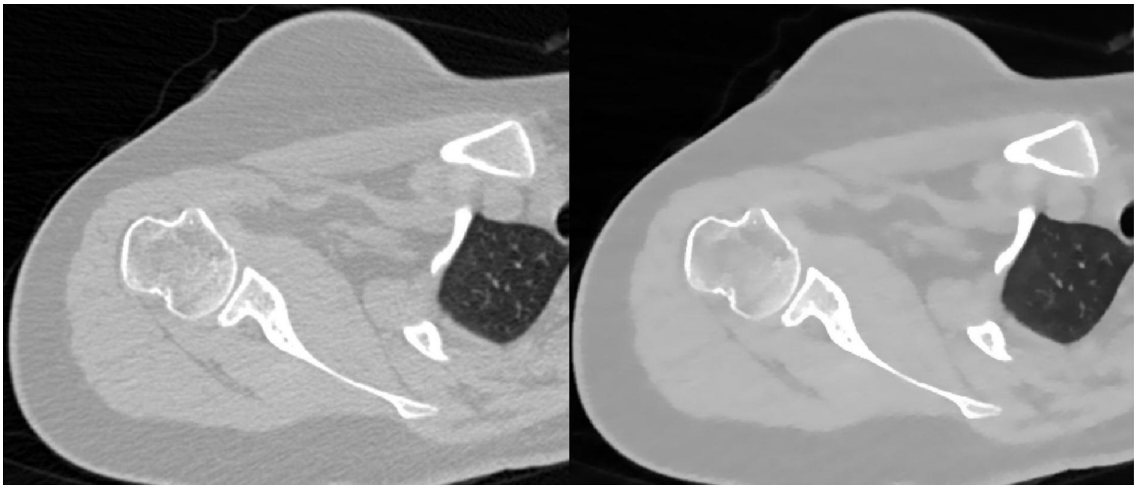

Figure 2.15 : Left, the original image form a CT scan of a shoulder joint, Right, bilateral noise removal method filter applied.

pixels. The second criterion is defined in the intensity domain, where pixels with closer intensity values get higher weights. By combining these two criteria, pixels with closer spatial distance and closer intensity values are assigned higher weights, while pixels which are spatially close but have very different intensity values are not greatly considered in the averaging calculation. In this way edges of the image, which by nature have a strong difference in intensity on each side, are preserved in the averaging process. The Bilateral filter also creates some side effects. One of the effects is that contrast regions appear in the image and staircase effects can happen. This can create a cartoon-like image [45]. Gradient reversal artifact near the edges is the other side effect of bilateral filtering [46]. Two different improvements over the bilateral filter have been proposed to remove the gradient reversal artifact [47, 48]. In this specific application where the input image is a grayscale medical image which will be used to extract the bones from the rest of the tissues, the side effects do not create an obstacle in the bone detection process. Figure 2.15 shows how the bilateral noise removal method keeps the edges of bones in the noise removal process on an example CT scan image of a patient's shoulder.

2.5.4.2 Gradient anisotropic diffusion filter

Anisotropic diffusion filter is a method of noise removal that preserves specific features like edges in the image. This filter works by creating a scale space where a family of images are produced by applying a different number of diffusion on the original image.

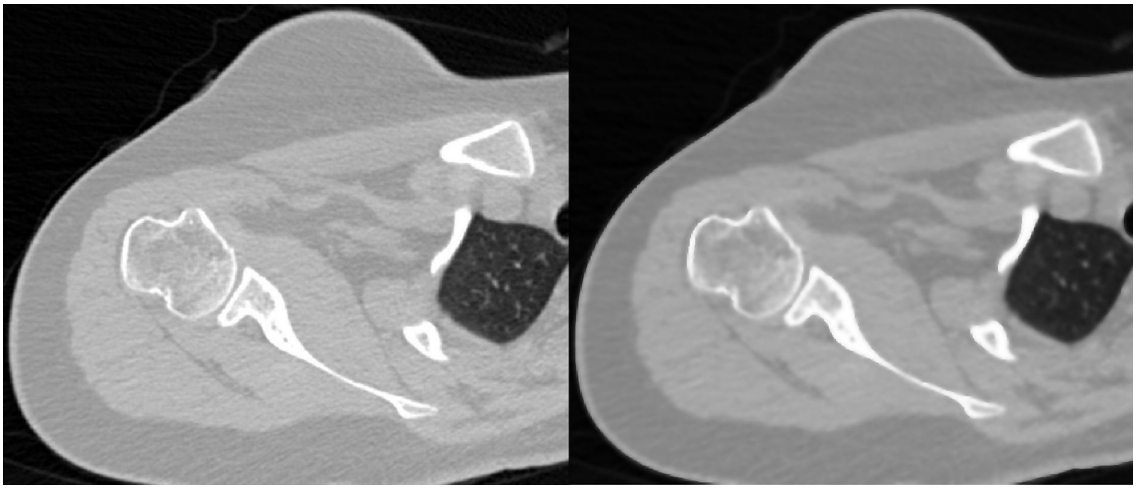

Figure 2.16 : Left, the original image form a CT scan of a shoulder joint, Right, gradient anisotropic diffusion filter applied with 20 iteration.

For each diffused image the diffusion parameter is different creating a different level of smoothing or noise removal on the image [49].

Unlike the isotropic diffusion methods that blur the edges where there is a big difference between the light and dark areas, an anisotropic diffusion filter uses the gradient of the magnitude of the image at each pixel which results in reducing the strength of diffusion at those points. Since each image in the family is created by applying the diffusion process to the previously created image and the gradient calculation helps saving the edges in the diffusion process, the process can be continued in each step until the needed level of noise removal is achieved while the edges and image features are still saved.

This filter has many applications in medical image processing fields specifically where noise removal is to be performed prior to segmentation operations. Figure 2.16 shows the result of a gradient anisotropic diffusion filter for 20 iterations versus the original image.

Anisotropic diffusion and bilateral noise removal filters have similar applications and the difference between them is that bilateral filter is a non-iterative filter while gradient anisotropic diffusion filter performs iteratively and involves partial differential equations [50].

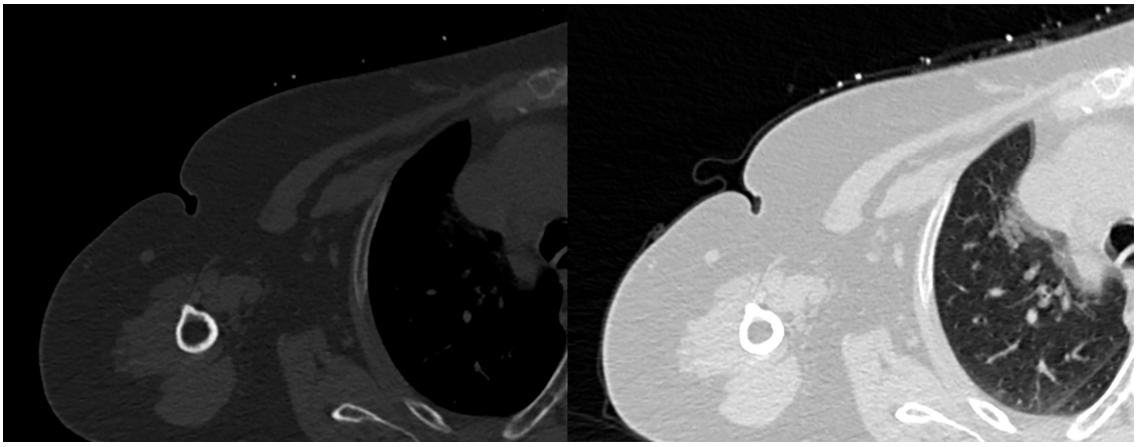

Figure 2.17 : contrast stretching applied to a CT scan image revealing the details in the data.

2.5.5 Contrast stretching

Contrast stretching is a technique that helps improving the data available in an image in cases where the data is compressed only in a small range of contrast values. The intensity values of the captured image that are being suppressed in a limited range make the data less useful and decrease the amount of details understandable from the data. Linear contrast stretching involves in finding the lower and upper limits of the intensity values and then mapping the data in between the limits to the whole range of data. Linear contrast stretching is the one used in medical applications to preserve the original information available [51,52]. Figure 2.17. shows how contrast stretching can reveal the details of the image.

2.5.6 Segmentation

There are different methods for the segmentation of parts of images in the literature. Thresholding, region growing, classification, clustering, and using deformable models, are among the most used methods [53]. Thresholding methods segment the image by using a threshold value in intensity for dividing the pixels in the image into different categories. Using one or more threshold values, pixels with intensity values bigger than the threshold will be categorized as another section from the pixels with intensity values less than the threshold value. The threshold value can be decided manually or can be obtained automatically using different methods [54]. Region growing techniques extract image regions which have pixels connected together by specific criteria. Similar intensity value, color, or texture are among the criteria for

region growing methods [55]. Region growing segmentation starts by choosing a seed point as the starting point and checks the connectivity of neighboring points by using the given criteria, and either accepts or rejects the neighbors to the current segment. Classification and clustering are among machine learning methods of image segmentation. In these methods, a feature space is derived from the image in which the partitioning is performed. The feature space in its simplest form can be the image intensities themselves [56]. In Classification, previous examples of the desired object to be segmented have been observed by the machine, and their properties in the feature space have been extracted. The segmentation operation compares the extracted features of the new object and the previous examples and decides if the new object can be categorized in the current class. Clustering is different from classification in that no previous example is provided for the evaluation and the definition of classes is extracted as the images are being evaluated. Object classes are determined in such a way that in each class objects have high similarity values, and objects of different classes are low in similarity measures [57]. This method is hence called as an unsupervised segmentation method. Deformable models use curves in two dimensional applications, or surfaces, in the case of a three-dimensional data, located in an image which can move. The motion of the model is influenced by two types of forces defined on the model. The first force is the internal force acting within the curve and trying to keep the curve smooth while deforming. The second force is the external force calculated from the image data and tries to push the model towards a specific form or shape [58].

2.5.6.1 Marching cube

Marching Cube is a method for extracting and segmenting an isosurface in multidimensional data which is the most popular method for isosurfacing [59, 60].

The basic working principle behind the marching cube algorithm can be described as below. The three-dimensional space of the medical image, which has an intensity value at each point, is divided into different cubes, with each cube having eight neighboring pixels of the image at its corners. All the cubes are evaluated for their corners intensity values. The cubes which have some corners with intensity values in the range of the bone intensity value and some other corners with intensity values outside the bone

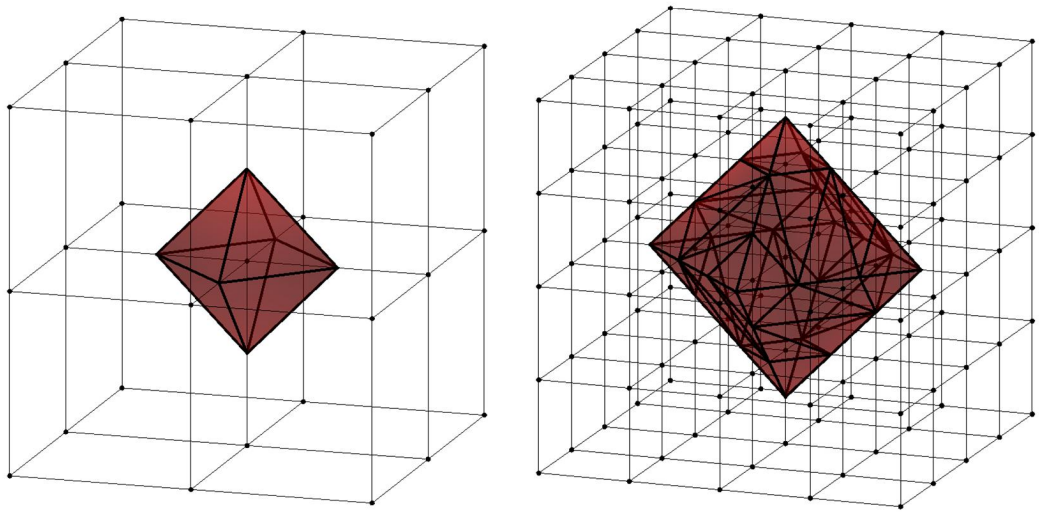

Figure 2.18 : An example of marching cube algorithm showing how intersections of each cube is found with two different resolution samples.

intensity value, are the cubes which the isosurface will pass through. On these cubes, intersection points are found on the edges which have one corner inside and the other corner outside the object. The surface will pass through the middle of the edge with points inside and outside. Next, a surface is drawn in each cube which connects the intersection points. Connecting all the surfaces in all cubes makes the total isosurface. Figure 2.18 shows an example of the marching cube algorithm at different resolutions.

2.6 Similar Works

There are several commercial PSI systems available that can be used in an operation but the computer techniques and tools used to develop such software packages are not fully presented in academic literature, because of trade secrecy.

Walch et al [17] describe very briefly the 3D model reconstruction and the definition and semi-manual measurements of some glenoid properties, as the initial steps for developing Glenosys PSI software, without explaining the programming methods used. In another study on the same software, Moineau et al [61] mention a method for manually selecting some points on the glenoid contour and then they define parameters for 3D measurement of glenoid morphology.

PSI software Signature TM glenoid guide system is discussed in two different studies [25, 62] where the research focuses on the usage and outcome of the software without describing any of the underlying programming tools.

Similar studies are performed to measure the application and accuracy of Surgicase Connect software [13, 23]. In these works as well, the software generation processes are not described.

By the use of Orthovis preoperative planning software for a reusable PSI guide, the implant positioning improvement is studied in [63]. The paper describes the planning procedure but the development of the software is not explained.

Cabarcas et al use a combination of commercial software tools and a C++ custom program to create a PSI for glenoid pin placement [64]. The information about software development is not given.

Other techniques have also been used to improve the accuracy of the guide pin or glenoid component positioning in shoulder arthroplasty.

Navigation systems provide the surgeon with a visualization system that aids placing the tools on the correct position by real-time displaying of the tool and the body parts. They use real-time tracking systems that follow the location of markers representing the tool and references on the body. Transformations then are calculated and updated real-time with a high rate to create an accurate display of the pose of the tool relative to the body parts.

Similar to PSI, navigation systems showed better accuracy than those of standard methods. While PSI requires time for preoperative planning and guide manufacturing, navigation systems can be more complex and require extra effort and time for calibration, reference frame positioning, and real-time tracking of components [8, 65].

Augmented reality (AR) is a new surgical assistance method that could improve RSA outcomes by providing visual information at the time of surgery and enabling remote interactions between surgeons [66, 67]. This method uses real world augmented with virtual world information like imposing virtual bone models on top of the real patient body. AR systems must be able to do three basic features. Combining the virtual and real world, the ability to create real-time interactions, and the ability to register the virtual and augmented objects accurately.

3. SOFTWARE DESIGN AND DEVELOPMENT

In this chapter steps in developing the 3D preoperative planning software for shoulder, arthroplasty is described. Techniques and libraries used for each step, the preoperative planning method, and the GUI of the software are explained.

The overall processing steps of the software and the order in which the PSI guide is created from the initial raw information is displayed in Figure 3.1. The first step is reading and importing input images, followed by pre-processing of the imported data. Detection of the bones among other tissues and then separating the scapula from the other bones are the next two steps. After having the scapula separated, the glenoid surface and specific landmarks are detected. At this stage, enough information about the scapula anatomy is acquired and the implant baseplate model placement into the 3D virtual space, and the preoperative planning is supported by the software. Next, the PSI guide design is created using all the information from the previous steps. The guide model is exported and ready for manufacturing so it can be used in the surgery.

3.1 Reading and Importing Patients' Data

Importing the data is the first step in the process. The data is captured using Computed Tomography (CT) scan. Digital Imaging and Communication in Medicine (DICOM) standard protocol is used to handle data communication between different commercial equipment regardless of their type and manufacturer. A specific image acquisition protocol is also created and used for capturing the CT data so that automatic data processing algorithms of the software can work flawlessly.

The CT scan acquisition protocol parameters defined and used in this work are as follows: 120 kV, 0.75-mm thick axial slices, pixel spacing of 0.53, and an image matrix of 512 x 512. These parameters are kept constant throughout all the parts of the study and form a standard for the software.

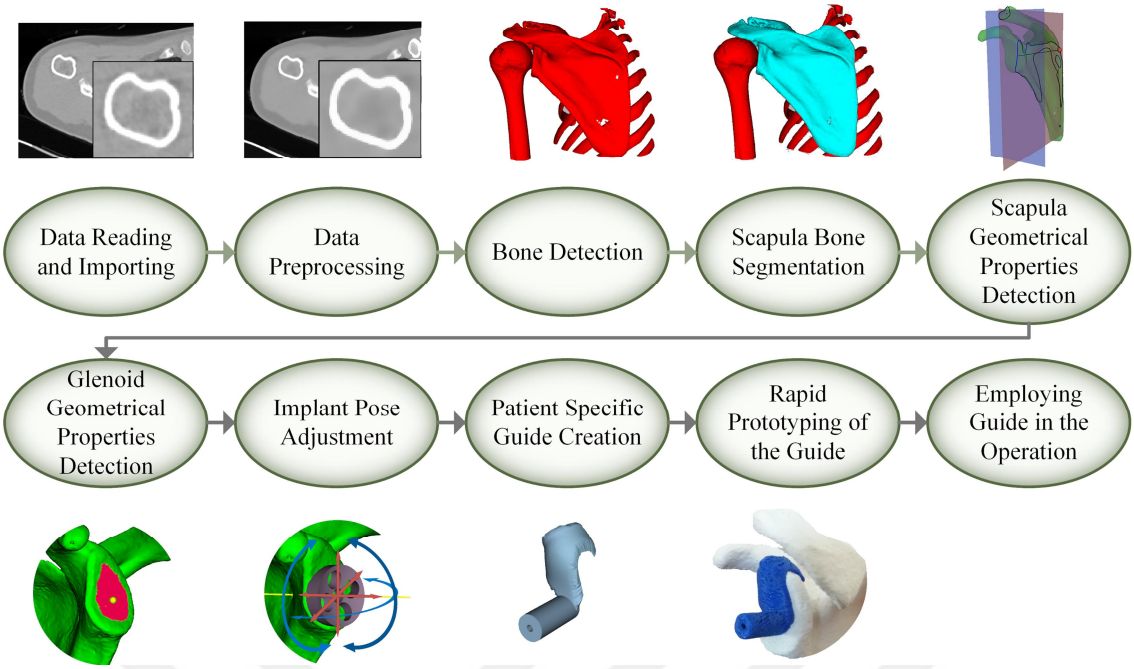

Figure 3.1 : The overall processing steps of the software and the order in which the PSI guide is created.

Grassroots DICOM (GDCM), which facilitates the reading and writing of DICOM images, is used for importing and sorting source DICOM data files. Browsing the collection of files, the GDCM Scanner class is used for detecting the number of 3D volumes, slice thickness, and pixel spacing of images in each volume.

After having the 3D volumes found in the data collection, the GDCM Sorter class is used for sorting the imported data based on specifically defined tags. Sorter class Implements a sorter using Image Position along the Image Orientation direction. Two tags used as a base for sorting are “study instance UID” and “Series instance UID”, which separate series in each study.

GDCM IPPSorter class is used for extracting the ZSpacing of 2D images from the patient position. It uses the sorted results from the previous step as the input and computes the spacing in between the layers of 2D images.

The Visualization Toolkit (VTK) is used next. The output of the IPPSorter class is used by the vtkImageReader class, a source object that reads DICOM files, in sorted order. The ZSpacing calculated from the data collection is still not applied at this step. vtkImageChangeInformation class is used to modify the spacing as part of the information accompanying the image data object created in the previous step without

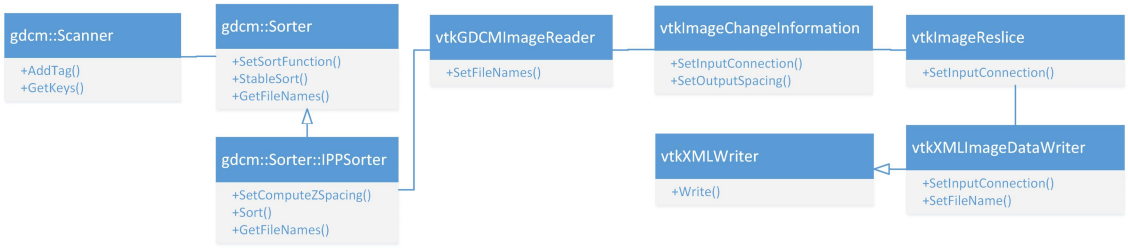

Figure 3.2 : The relationships between the classes and implemented functions used for reading and importing patient's data.

changing the data itself. Using the modified information, vtkImageReslice resamples the image volume along the Z axes. In this step, the image object ZSpacing is correctly applied.

Using vtkXMLImageDataWriter Class which is a subclass of vtkXMLWriter the image data is saved to a file to be used in the other steps of the program. Figure 3.2 shows the relationships between the classes and implemented functions.

3.2 Pre-processing

Medical images corrupted when acquired through a CT scan need to be improved before they can be used in other steps. CT scan images can capture a wide range of intensity values but the existing intensity values in the images can be limited in a specific range. Contrast stretching is used to bring the information in the images to a broader grayscale range.

After contrast stretching is performed, noise removal must be applied to the image data. The noise reduction method used must preserve the features of the images so that the geometrical accuracy of the three-dimensional model extracted from them has high accuracy. A bilateral noise removal filter preserves the edges in the images which will keep the bone shape accurate and is used in this work.

Gradient anisotropic diffusion filter is another method for edge-preserving noise removal. Different implantations of these algorithms are available open source for C++.

Insight Segmentation and Registration Toolkit (ITK) is used for applying noise removal filters to the image data. ITK BilateralImageFilter and ITK Gradien-

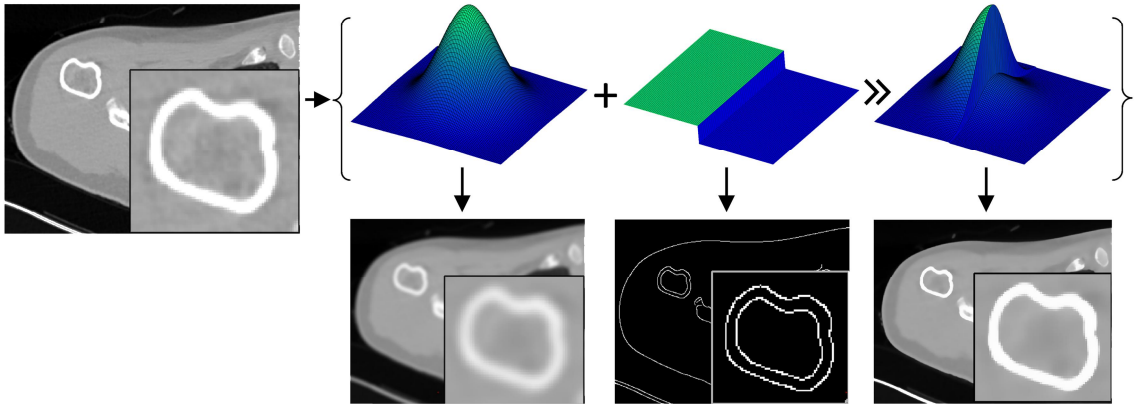

Figure 3.3 : Bilateral noise removal filter applied to a slice of CT scan data of a shoulder joint.

tAnisotropicDiffusionImageFilter are the implementations of these methods used in this work for their efficiency and good documentation. Figure 3.3 shows bilateral noise removal filter applied to an slice of CT scan data of a shoulder joint

3.3 Bone Detection

The marching cube algorithm is the most successful isosurface extraction algorithm which is simple to implement, and as a result, to detect and separate bones from other tissues in the data, a marching cube algorithm is used in this work. Marching cube uses a threshold value to extract an isosurface from a three-dimensional scalar value dataset. To automate the application of the marching cube on 3D image data, the threshold value must be chosen by the program. Incorrect threshold value either leads to including other non-bone tissues in the bone model or excluding important regions of the bones (Figure 3.4). Information existing in the DICOM header section including CT scan protocol, and patient's data (age, sex), and the fact that the Hounsfield unit in CT is proportional to the degree of X-ray attenuation in different tissues [68, 69] are used to enable the algorithm to extract a suitable threshold value automatically.

3.3.1 Scapula bone detection

The scapula needs to be separated from other bones so that other feature detections can be applied to it. To do this segmentation proper criteria must be used. The geometrical properties of the scapula and other bones existing in the data in this specific part of the body offer the use of the surface area as a parameter. The scapula has the largest

Figure 3.4 : Segmentation of bone from other tissues of the body and segmentation of scapula from other bones. Middle images show the incorrect threshold value effects on the segmentation.

surface area among all other bones in the data frame. VtkPolyDataConnectivityFilter is used to calculate the largest region in the bone model and then separate it from other regions (Figure 3.4). After this step, the model of the scapula bone is accessible to the algorithm as a separate object.

3.4 Scapula and Glenoid Features Detection

After separating the scapula in a new object, certain features of it must be determined. Some of these features are necessary for the automatic operation of the algorithm on patient-specific guide design. Some other features are required to provide the user with proper information so that they can make a better decision on the final pose of the implant.

At first, the position and orientation of the scapula model in the 3D space of the image must be determined. To understand the position and orientation of the scapula in the 3D space of the model, the scapula plane, glenoid plane, and medial axis are to be found. Having these features will completely define the position and orientation. To find these features, special scapula geometrical properties are used. These geometrical properties demand the two most distanced points on the scapula to be located; one close to the inferior point of the scapula and one on the outer side of the acromion. These points are found by calculating the distances between all pairs of points on the scapula isosurface model and selecting the points that create the maximum distance value. After having this pair of points, to find out which of these points is the inferior point, the curvature value of two the points is compared. The inferior point has a much higher curvature value since it is located on the very bottom of the scapula body. The

other point on the outer side of the acromion is located on a more flat surface and has a lower curvature value.

To find the curvature of those points, the curvature value of all points on the scapula surface is calculated using the vtkCurvatures class. There are four different options for calculating the curvature value using this class namely; Gaussian, mean, maximum, and minimum. For this program, the maximum method of computation option is used.

To find the glenoid surface of the scapula, first a point on the glenoid surface must be found. Two different methods have been explored to find this point. The first method tries to find it by first finding the orientation of the glenoid plane and position of the glenoid surface edges, and then passing a line through the glenoid plane inside the edges to find an intersection point.

To find the glenoid plane, first 3D visualization of the model of the scapula is used to create two dimensional projections from different orientations. This is done by rotating the 3D model of the scapula in small angles and taking 2D projection images in each step. The rotation is performed around all three axes so that the scapula is viewed thoroughly from all angles. The position of the center of rotation is decided by averaging the position of all the points on the scapula.

In the next step, an edge detection method is applied to two dimensional projections to detect the edges. The edges in the projected images show the periphery of the bone. The edge patterns resulting from the previous operation are compared to a reference image containing the edge pattern of the general shape of the glenoid. (Figure 3.5).

The approach to perform this comparison is to compute the correlation coefficient between the two images. The correlation coefficient is a quantitative similarity measure between the two images. The higher the correlation coefficient, the more the two images match each other. This operation is repeated for all of the two dimensional projections and the highest correlation factor value decides the closest projection to the reference image. This projection defines the orientation of the plane parallel to the glenoid surface. (Figure 3.6)

Parameters affecting the speed, accuracy, and repeatability of this method are evaluated. The speed of the operation is affected by different parameters including the hardware used, the resolution of the input images, and the algorithm itself.

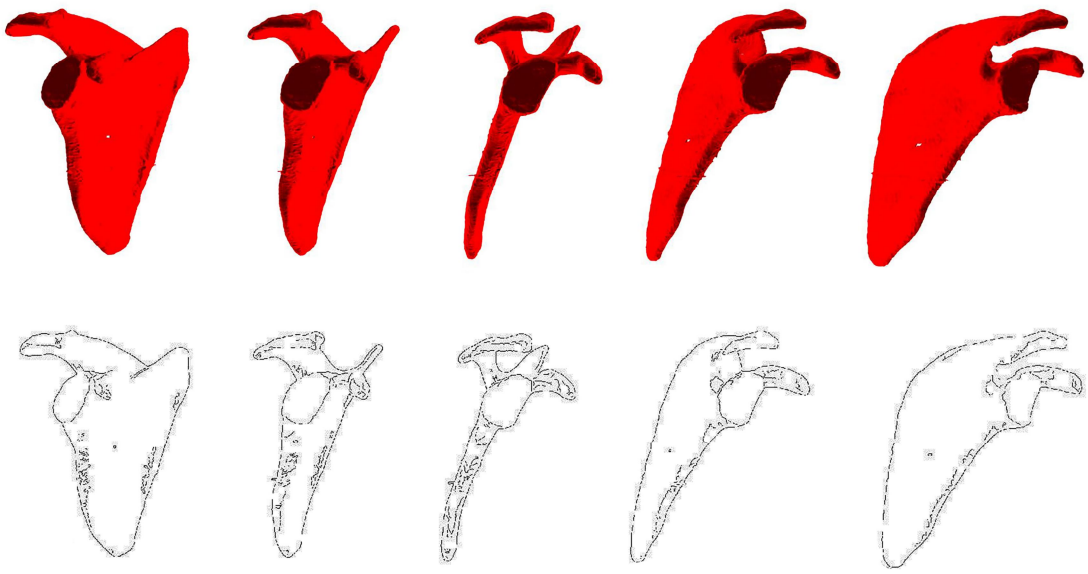

Figure 3.5 : 3D model of scapula rotated and the edge patterns detected for each rotation.

The 2D image resolution has a twofold effect on the algorithm. If the resolution is higher, the algorithm takes a longer time to complete, but at the same time, it can improve the accuracy of the algorithm by including more accurate input data.

The rotational resolution, or the resolution of rotation angles in between every two dimensional projection, is another factor affecting the speed of the algorithm. The higher the rotational resolution, the more 2D projections are created and the slower the total process. Keeping the rotation resolution low, increases the speed of the algorithm, however, this can have a negative effect on the accuracy of the method. When the rotational resolution is increased or the angle in each rotation is decreased, more projections are created which provides a better chance to detect the most precise orientation, which has a negative effect on the speed of the algorithm.

The solution applied to this issue is to apply a fine-tuning step after finding the initial result. In this way, using a lower rotational resolution with higher speed, the algorithm finds an initial orientation close to the optimal one. In the next step, the algorithm is run again to create 2D projections and analyze them to find the highest correlation, but this time projections are made only in a close range around the initial result. In this step, the resolution can be much higher than the first step. Using this method the algorithm performs a fast and precise operation.

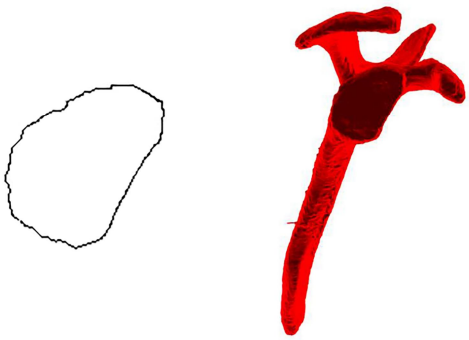

Figure 3.6 : The reference image containing a general pattern of glenoid surface edges, and the final orientation of glenoid surface detected by the first method.

Since the algorithm performs analysis on 2D images taken in discrete angle intervals, the initial orientation of the scapula bone in the three dimensional space can affect the orientation detected as the initial result and affect the repeatability of the method. This effect can be minimized through the fine-tuning step of the algorithm. A higher rotational resolution in the fine-tuning step will result in minimizing this effect. The results of this method were not satisfying when applied to different cases and a good generalization was not achieved.

The direction of the lighting in the rendering of the scapula 3D model has an important effect on the result of this method. Depending on the relative location of the lighting source with the camera position and the center of rotation of the model, the shade appearing on the glenoid surface changes. This change affects the edge detection result which can make the algorithm unsuccessful. A more important obstacle for this method is found to be the diversity in the shape of the glenoid surface between cases. This diversity makes it very difficult to have a general glenoid surface shape to be used as a reference.

The first method mentioned for finding a point on the glenoid surface is rejected for the study and a second method is used. The second method uses the two points found in previous steps, one the inferior point of the scapula and one on the outer side of the acromion. A line that passes through the two points, intersects with the glenoid surface (Figure 3.7(a)). This intersection point is found and then used as the seed point to find all the points on the glenoid surface. Since the shape of the glenoid surface has a central curved surface that is limited to the sharper edges on the outer perimeter, a

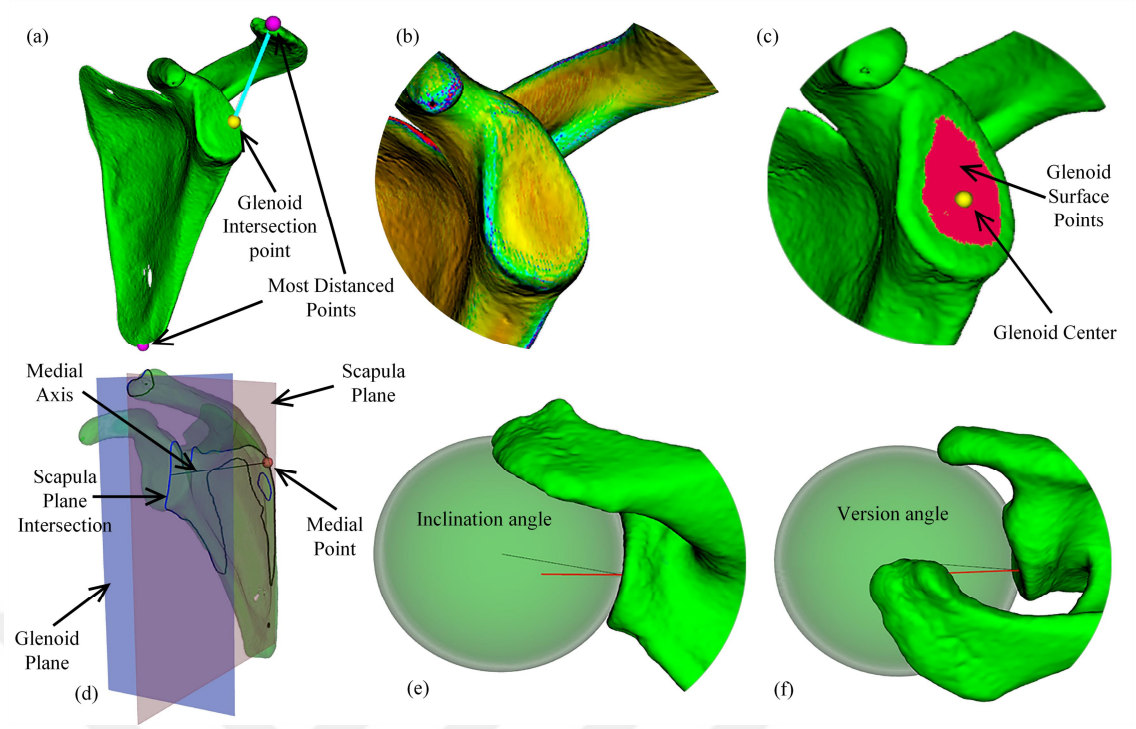

Figure 3.7 : Different features of scapula bone and the glenoid surface used for algorithm development.

curvedness-based region growing algorithm is used to detect the points on the surface from the other points on the scapula surface [70].

This algorithm starts from a seed point and iterates on the neighbors of that point and adds them to the surface if they are within a certain threshold of curvature value. Next, the same process is iterated for all the points that currently belong to the glenoid surface points. In this way, the surface region of the glenoid grows on each iteration until it has reached the edges of the glenoid where the curvature value of voxels increases to a value higher than the max threshold value (Figure 3.7(b)).

The glenoid center point is found by averaging the coordinate positions of all points of the surface and finding the closest point to it that is located on the glenoid surface (Figure 3.7(c)). For damaged scapula bones with a fractured glenoid surface, where the line connecting the two most distanced points does not intersect with the glenoid surface, the software asks the user to select a seed point on the intact section of the glenoid surface. This part of the algorithm then works semi automatically using input from the user for these specific cases.

To find the scapula plane three points are needed. The inferior point of the scapula, the glenoid center, and the center of weight of all points on the scapula surface, comprise these three points. The inferior point of the scapula and the glenoid center point are found in previous steps. To find the medial point of the scapula, first, the intersection of the scapula plane and the scapula model surface is found. This intersection is in the form of a contour line, which passes through the glenoid center, and the inferior point of the scapula. On this contour line, the point which has the furthest distance from the line connecting the glenoid center and the inferior point of the scapula is the medial point of the scapula [71]

After having the medial point, the medial axis is found by connecting the glenoid center and the medial point. At this point, the glenoid plane can be found as a plane that passes through the glenoid center and has the scapula medial axis as its normal (Figure 3.7(d)).

The glenoid normal is defined as the line connecting the glenoid center to the center point of the best fit sphere to the glenoid surface [61]. The sphere fitting algorithm works by minimizing the least square error in the sphere center distance to all the glenoid surface points.

Inclination and version angles can be found at this point using the other features. The inclination is the angle between the glenoid normal projected on the scapula plane, and the scapula medial axis (Figure 3.7(e)). The version is the angle between the glenoid normal and the scapula medial axis when they are projected on the transverse scapular plane (Figure 3.7(f)).

3.5 Graphical User Interface

GUI of the software is designed considering that it must provide enough tools for the user to provide them a convenient preoperative planning experience, and simultaneously present required information about the joint and anatomy to facilitate decision making for the surgeon.

The Graphical User Interface (GUI) of the software is developed using Qt designer with Microsoft Visual Studio 2015 C++ compiler. As the software uses VTK for

rendering, the VTK renderer object is linked to the Qt renderer to be displayed on the Qt designed interface.

The GUI is designed to have three main sections as is shown in Figure 3.8. In the left section of the graphical user interface, two-dimensional slices of the scapula bone of the patient are displayed in axial, medial, and coronal view orientations. These two-dimensional images are sliced from the scapula bone at the scapula plane, glenoid plane, and transverse scapula plane, and show the inner structure of the scapula bone. The boney parts are displayed in a different color than other tissues for better visualization. Zooming and panning operations can be applied to any of the two-dimensional views independently, in case a closer inspection is needed on a section of the bone.

The central section of the graphical user interface displays the three-dimensional scapula bone model. In this section, the preoperative planning steps' results are observed and manipulated. Different features of the bone model can be observed when activated. When any of the features are activated, the rendering of the model is updated so that the feature is added to the scene, and likewise, when the feature is deactivated the scene is updated again. Like the two-dimensional sections, zooming and panning operations are applicable to the model in this section, so that the surgeon can inspect any section of the bone more accurately. Rotation of the model is also available in this section which is not the case for the two-dimensional views. On the top side of the rendering section, standard orientation buttons are located so the user can easily look at the model from these predefined angles.

The right section of the graphical user interface is the main control panel where different features of the software, as well as planning operations, are controlled.

On the top side of the right section, the patient's information is given and visualization of the three-dimensional model is controlled. Activation and deactivation of the scapula bone's model's features are performed in this section. These features are as follows: the scapula plane, the glenoid plane, the medial axes of the scapula, the best-fit sphere to the glenoid surface, and the glenoid normal. The scapula bone transparency and its amount also can be controlled here, to provide better visualization of other

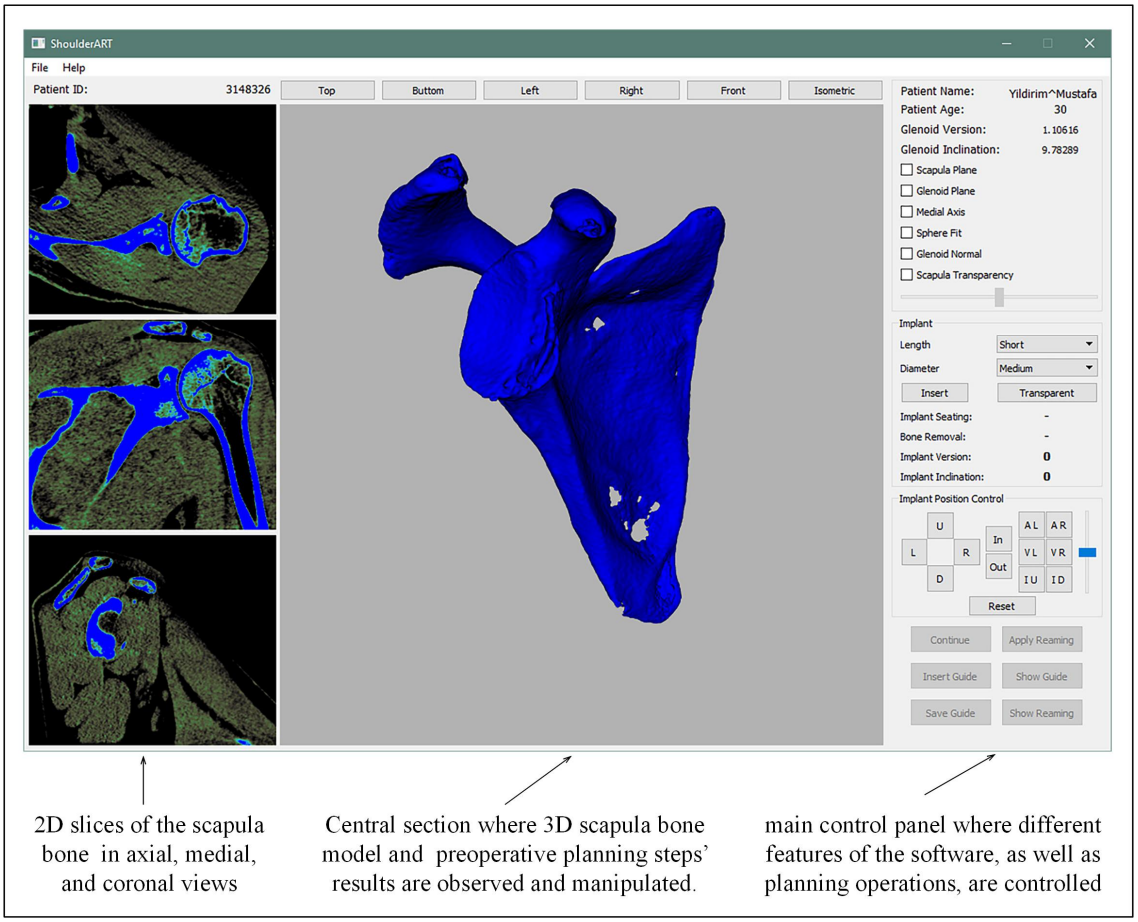

Figure 3.8 : Different sections of the GUI of the software.

features. In this section, geometrical information of the glenoid, including inclination and version, is also displayed.

The other subsections in the right section of the graphical user interface, are designed to enable the user to perform the preoperative planning steps.

Implant model insertion to the 3D model of the bone and its properties are controlled in the implant subsection. The orientation and position of the implant inserted relative to the scapula bone is controllable in the implant position control subsection. If the software is able to create required guides' models based on the bone and implant geometrical conditions, then many of the factors which are decided during the surgery can be decided preoperatively which is a big help in reducing operational risks. Below these subsections, buttons are designed to perform and advance different steps of the planning procedure to help with the creation, insertion, and saving of the guides to be used with the specific implant.

3.6 Software Assisted Preoperative Planning

The steps and processes that are designed to be performed for planning using the software are described in this section. The Very first step for using the software by a surgeon after opening it is to choose the folder contacting the DICOM files of a patient. After that, the software does all the operations required to prepare the scapula bone model and display it on the GUI.

The surgeon then will evaluate the bone model. He or she has access to reorienting tools to look at the scapula model from different viewpoints. Mouse interactions in 3D space provide zooming in or out, panning, and rotating motions. The surgeon can use features available in the GUI to better observe the bone properties like scapula plane, glenoid plane, medial axis, sphere fit to the glenoid surface, and glenoid normal. The transparency of the bone can also be adjusted during any step of the planning.

Evaluating the 3D model of the scapula gives the surgeon a good understanding of the specific conditions of the bone. In this step of the process, the software is ready to be used for the insertion of the implant to the specific patient bone model by the surgeon. The surgeon selects an implant baseplate type and size from the implant selection menu of the GUI and commands the program to insert the baseplate model. The predefined

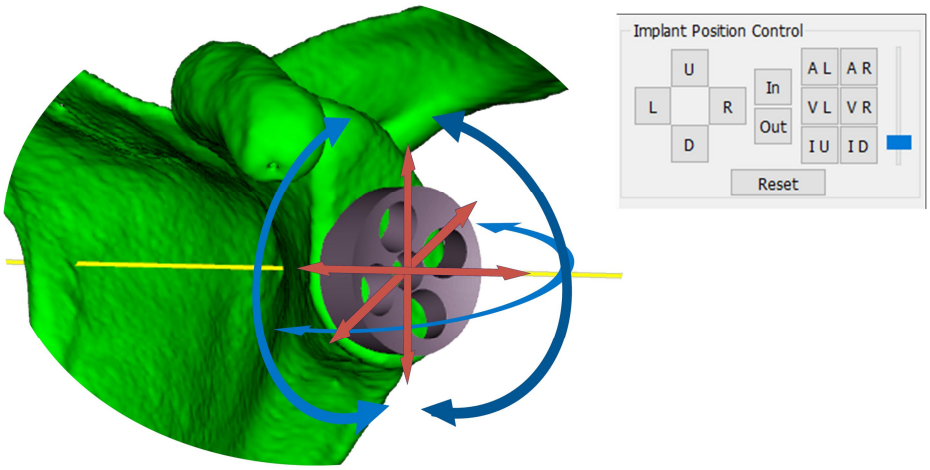

Figure 3.9 : Implant baseplate inserted on the Glenoid surface and the adjustment that can be performed by the software user.

STL model of the implant baseplate is imported and displayed on the 3D space of the GUI. Initially, the baseplate is automatically located in a way that its curved surface sits on the glenoid surface and coincides with the glenoid center. The surgeon then can use the implant pose control panel to move and rotate it in all six degrees of freedom. Translations and rotations are performed on the implant's actor location with each button click in the GUI. The amount of translation or rotation in each button click is changed using a sidebar to provide the fast motions or small adjustments (Figure 3.9).

The transparency of both the scapula model and the baseplate model can be adjusted. The version and inclination angles of the implant are calculated and displayed on the GUI as the baseplate is moved. These angles are among the important factors for shoulder arthroplasty operation.

The amount of sitting of the baseplate on the bone and the amount of bone removal are other important factors in deciding the implant position which affects the stability and longevity of the implant [72–74]. This value is calculated as the number of voxels of the backside surface of the baseplate's model that is located inside the scapula base model, over the total voxels of the backside surface of the baseplate's model. This value is also instantly updated by the model's motion so the surgeon can continuously control its value. The amount of bone removal is calculated as the volume of the bone that is removed from the scapula during the reaming operation.

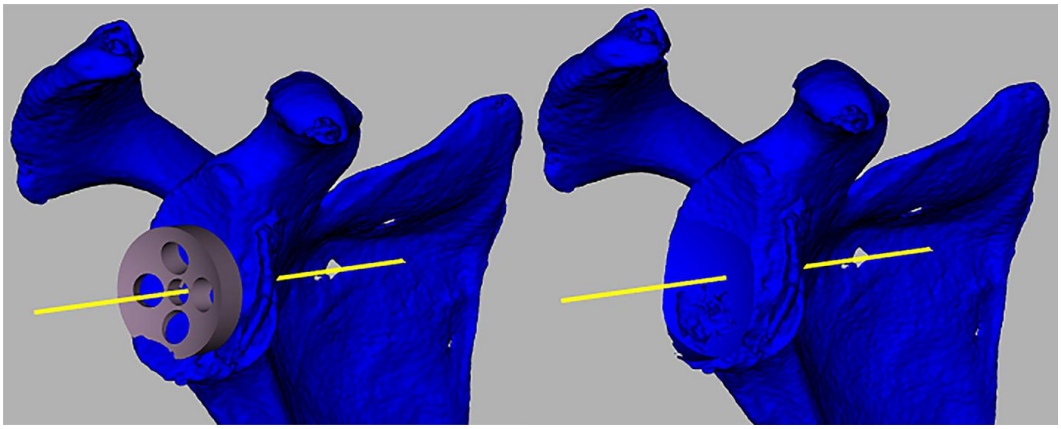

Figure 3.10 : The reamed glenoid is shown based on the defined position of the implant baseplate.

Changing the type and size of the implant baseplate is possible at any time during planning. Using these features the surgeon can optimize the pose of the implant to create the best results.

After the surgeon decides about the pose of the implant baseplate the reaming operation is applied to the scapula bone model. The reaming will remove some amount of bone from the glenoid surface so the implant baseplate can sit properly on the bone. The reamed bone is then displayed in the GUI. As shown in Figure 3.10.

At this point of the planning, the surgeon orders the software to create the guide for baseplate central hole drilling operation. This hole will be used as a reference and decides the implant's baseplate pose and the reaming tool pose. After the guide is created by the software it is shown on the GUI and the surgeon can evaluate the guide model on the bone model. Next, the surgeon will order the software to save the guide model to be manufactured and used intraoperatively.

3.7 Guide Design

The automatic creation of the guide is the next step after finalizing the pose of the baseplate by the surgeon. At this point, enough information is available for the guide creation. An important parameter in the guide design is proper seating on the glenoid surface in a way that it sits firmly and does not move during the drilling operation, and at the same time it creates a fixed position for the drilling operation. To meet these requirements the guide design firstly uses a shape that has a proper surface area

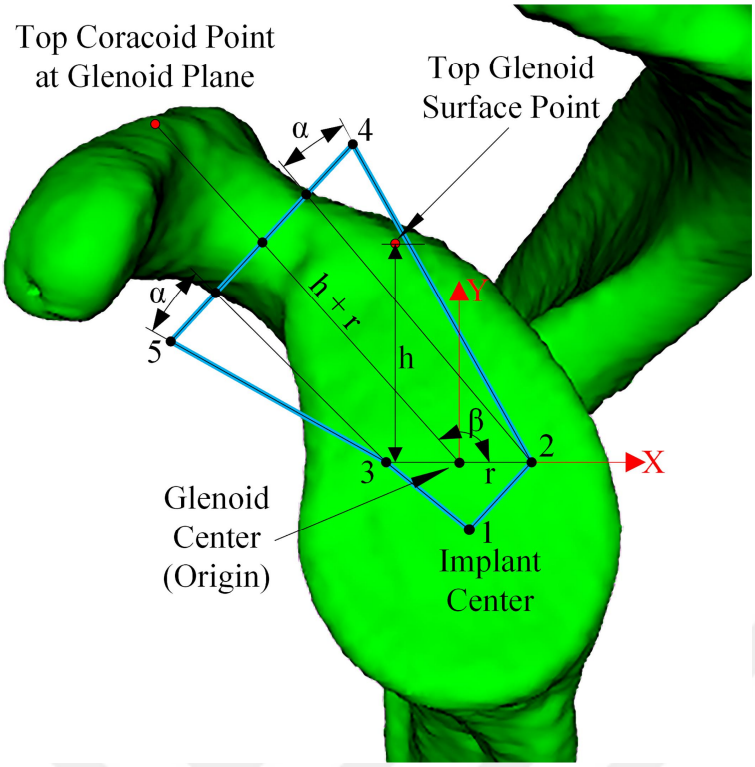

Figure 3.11 : Creation of initial 2D polygon on the glenoid surface.

for seating on top of the glenoid surface. Secondly, it uses the coracoid neck as a reference point for fixing the position.

The algorithm starts by creating a 2D polygon on the glenoid plane (Figure 3.11). The first point of the polygon is chosen as the implant baseplate center or the position of the drilling, which is already defined by the user when inserting the implant baseplate in the model. The next two points (points 2 and 3) are found by moving in positive and negative ways from the glenoid center point on the X-axis for a fixed amount. The fixed constant "r" is equal to the radius of the cylinder guiding the drilling tip. This value is set knowing the drill tip diameter and amount of material required to create enough strength for the guide.

To find the next two points, two reference points will be detected. The first reference point is the point with the highest y-value that belongs to the glenoid surface. The software already knows the points that belong to the glenoid surface. This geometrical feature is used to decide the dimensions of the guide to be created. The height "h" specified in Figure 3.11 is found as the vertical distance between this reference point and the glenoid center point.

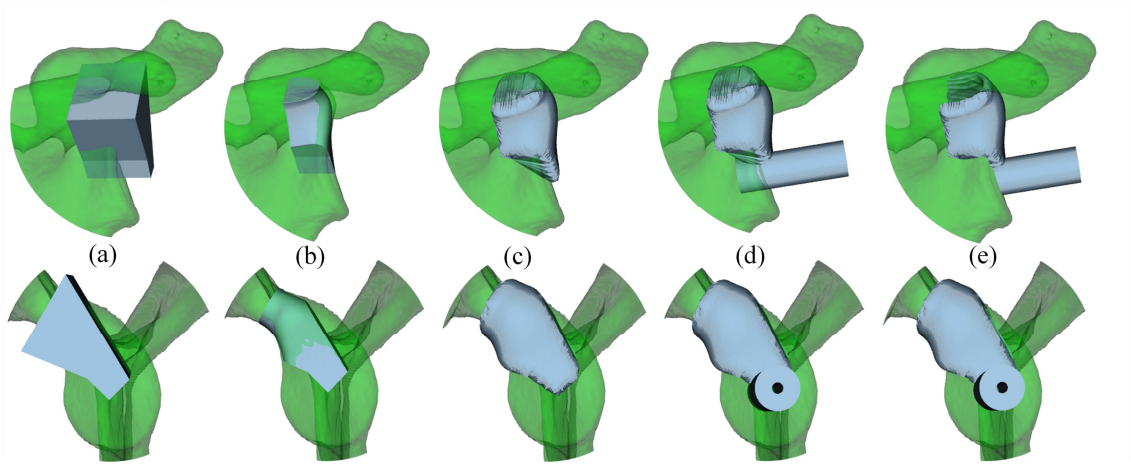

Figure 3.12 : Steps in creating the 3D computer model of the patient specific K-Wire guide.

The second reference point is the point belonging to the coracoid which is located on the glenoid plane and has the highest y-value in this plane. This point is used to find the direction where the coracoid is located in relation to the glenoid center. The angle β represents this direction and combined with the length (h+r) detected from the first reference points provides the required information to specify points 4 and 5 of the polygon. The angle α is a constant value that makes the guide design cover enough area around the neck of the coracoid. The angle α has a fixed value set manually in the software based on the evaluation of different scapula bone types. The following formulas give the equations to find the positions:

$$x_4 = (h+r)\cos\beta + r(\sin\beta)^2 + (h+r(1-\cos\beta))\tan\alpha\sin\beta \tag{3.1}$$

$$y_4 = (h+r)\sin\beta - r\sin\beta\cos\beta - (h+r(1-\cos\beta))\tan\alpha\cos\beta \tag{3.2}$$

$$x_5 = (h+r)\cos\beta + r(\sin\beta)^2 - (h+r(1+\cos\beta))\tan\alpha\sin\beta \tag{3.3}$$

$$y_5 = (h+r)\sin\beta - r\sin\beta\cos\beta + (h+r(1+\cos\beta))\tan\alpha\cos\beta \tag{3.4}$$

After having all the points which create a polygon, the polygon is extruded in the z-direction to form the first volumetric section of the guide (Figure 3.12 (a)).

Next, the intersection of this volume and the scapula model is found by applying the Boolean operation (Figure 3.12 (b)). This intersection volume is then wrapped outward (Figure 3.12 (c)). In this stage, a smoothing filter is applied to the wrapped volume.

The next volume that is added to the guide design by a union operation, is the cylinder that will guide the drill bit. The radius of this cylinder has a fixed value. The central axis of the cylinder passes through the point where the implant baseplate's center was located on the glenoid surface. The cylinder is oriented in a way that its axis has the exact orientation of the implant drilling orientation set by the software user during the planning.

After adding the cylinder, the center part of it is emptied by subtracting another cylinder with the same properties but a smaller diameter, to create the path for the drilling tip (Figure 3.12 (d)).

The last operation on the guide is removing the intersection area of the current volume and the scapula, which is performed by another subtraction operation (Figure 3.12 (e)).

The Boolean operations are performed using the CGAL library. To interface the mesh models between VTK and CGAL, OpenMesh library is used. Using OpenMesh, VTK's STL objects are transformed into Object File Format (OFF) format to be readable by CGAL and the transformation is reversed after the Boolean operation so the objects are imported to VTK again.

After the guide model creation process is finished, it is displayed on the GUI (Figure 3.13), located at its exact position on the glenoid surface. The guide created by the software is saved as an STL model. This model is used later for the manufacturing of the physical model of the guide.

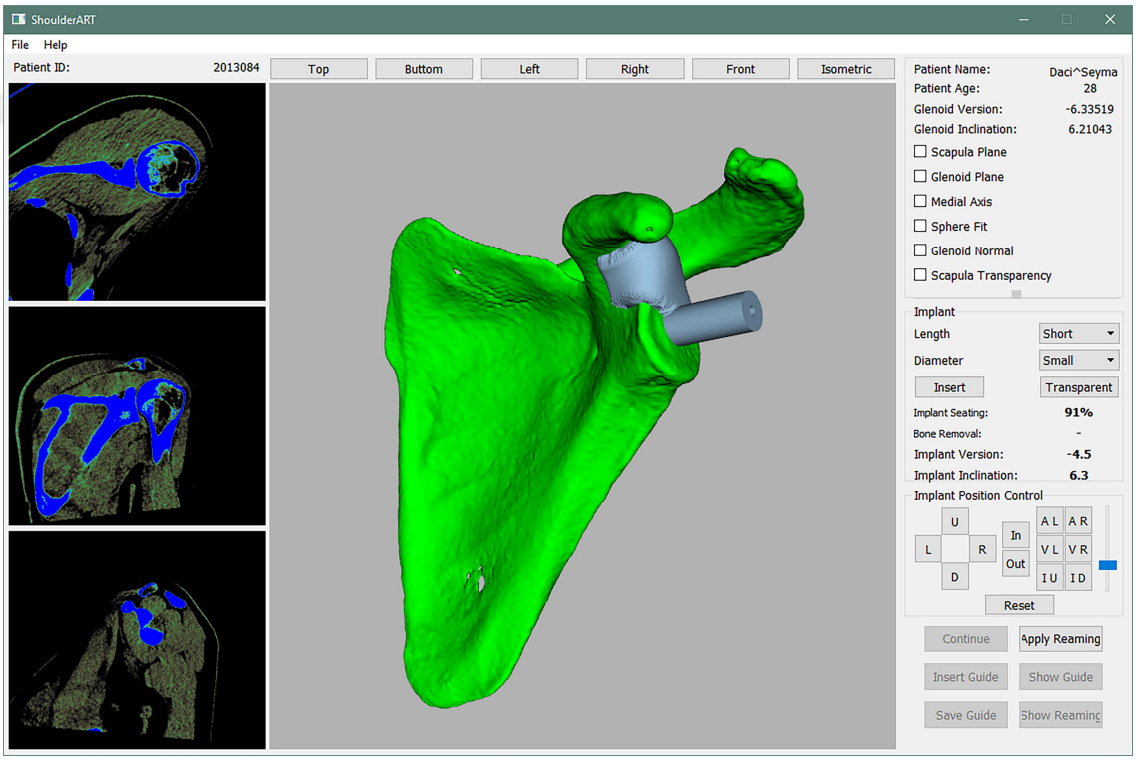

Figure 3.13 : Final PSI guide designed shown on the GUI of the software.

4. EXPERIMENTATION AND TESTING

Experiments were designed to test the software from different aspects. First to check the software capability for performing preoperative planning on different patients and observe the quality of guides designed. Second to check the accuracy of the results of the operations performed when preoperative planning is done by this software for different glenoid types. To reach these goals, the experiment used computed tomography (CT) scans of five different scapula types. As most glenoid deformities are related to osteoarthritis, the Walch classification was used to build the study groups. Based on the Walch classification one scapula each was type A2, B2, C, and D, and one scapula had an intact or non-arthritic glenoid. Based on the Favard classification the same scapula bones were categorized as E0 (non-arthritic glenoid), E1 (Walch types A2, B2, D), and E2 (Walch type C).

High-resolution imaging of the selected cases was performed with a pitch of less than 1 during CT scanning. The CT scan parameters were as follows: 120 kV, 0.75-mm thick axial slices, pixel spacing of 0.53, and image matrix of 512 x 512. After capturing the image data from all patients, the 3D preoperative planning was performed for each scapula by the surgeons, and the same planning was used for all methods. The guide models and the scapula bone models were saved to a computer after the planning.

4.1 Rapid Prototyping of the Bone Models and Guides

For the experiment to be performed, 3D-printing rapid prototyping of the scapula bone models was done using the Fused Deposition Modelling (FDM) method (Figure 4.1). The material used for 3D printing of the bone models and guides was polylactic acid (PLA).

A total of 150 full-size physical scapula models and 15 guide models were manufactured. The 3D printing was done with an Ultimaker 2 and an Ultimaker 2 extended Printers. The 3D printing parameters were optimized for printing speed while keeping the level of details acceptable for the experiment. The total printing time was

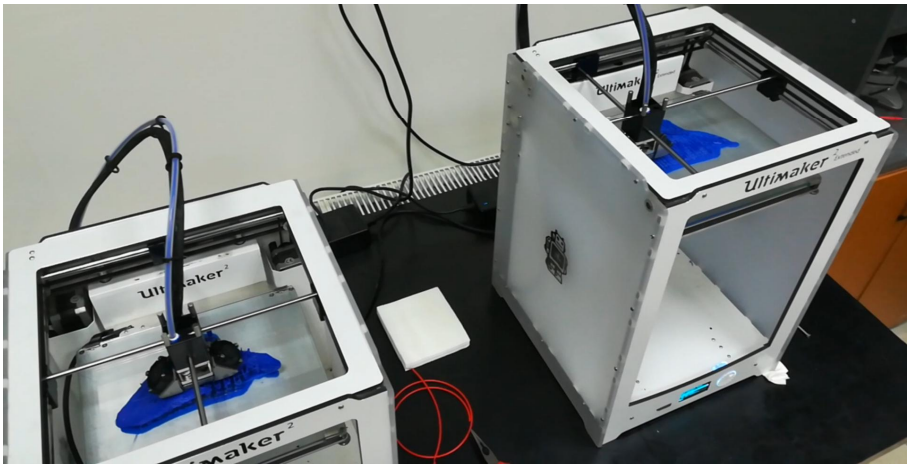

Figure 4.1 : Manufacturing of the scapula bone models using rapid prototyping technology.

around 750 hours by both machines. Supports were used for printing the scapula models because of the special shape of the bone, and the supports were manually cleaned after the manufacturing.

4.2 Experiment Method

The bone models manufactured were labeled and coded. For each group of scapula type, the experiment was performed using three different methods, and each method was repeated five times by two different surgeons. The experiment was performed 30 times for each group, making a total of 150 tests.

A specific room was dedicated in the hospital to set up the experiment. Fixtures were set up to hold the scapula bones.

The first method of the experiment was the freehand technique. In this technique, the surgeon does not use any guide to positioning the guide pin for the glenoid baseplate. The surgeon first marked the inferior circle of the glenoid surface on the bone and determined the entry point of the guide pin without any helping device and based on his experience. Then he performed the drilling of the guide pin into the bone based on the marking.

In the second method, the surgeon used an RSA conventional non patient-specific glenoid guide with a predefined angle to guide the guide pin. The surgeon placed the guide flush to the inferior rim of the glenoid cavity. This guide position and the

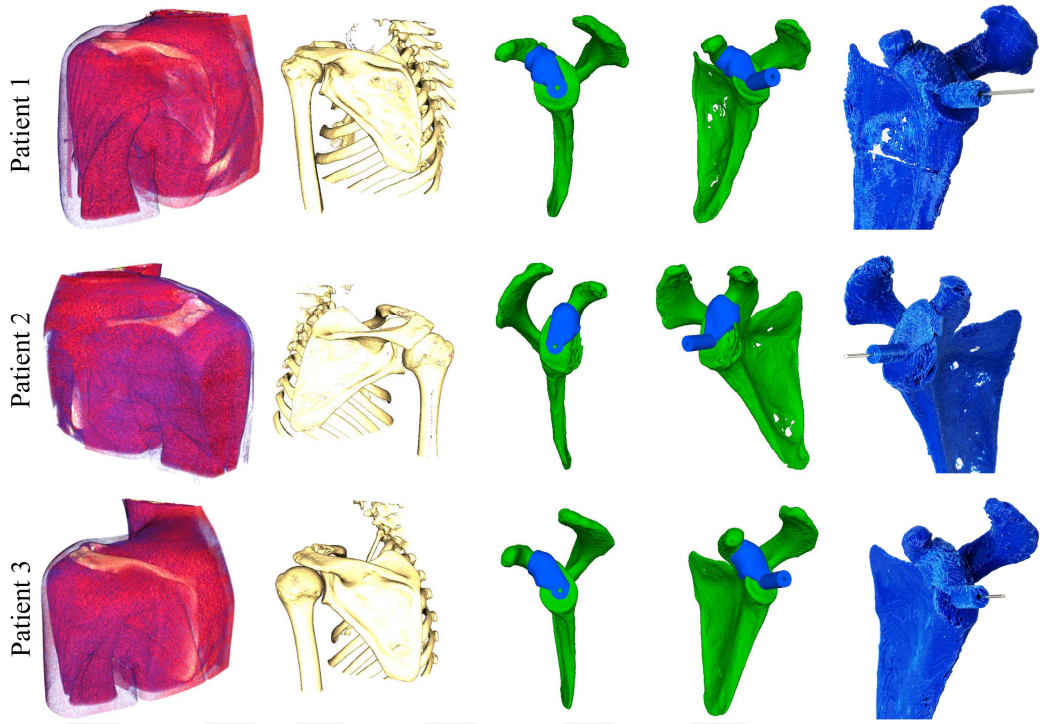

Figure 4.2 : Three patients' initial data, designed guides by the software for each patient, and K-wire inserted to the scapula bones by the surgeon using guides manufactured by rapid prototyping.

central hole with a 10° inclination allow the possibility of the appropriate placement of the central guide pin.

The third method of the experiment used the guide created by the PSI software developed in this study. It had an exact position for the guide pin and sat tightly on the glenoid area in a specific predefined position. The surgeon first installed the guide on the glenoid surface and then performed the drilling of the guide pin using the PSI guide. In Figure 4.2, three patients' initial data, designed guides by the software for each patient, and K-wire inserted to the scapula bones by the surgeon using guides manufactured by rapid prototyping are presented.

For the freehand and the conventional guide methods, models were covered by aluminum foil, and only the glenoid cavity of the model was visible to the surgeon during the experiment, to simulate the surgeon's view of the scapula bone in a real operation (Figure 4.3). The different scapula models were randomly mixed and the surgeons were blinded to the randomization. Operation using the PSI guide was performed after the other methods and other sections of the scapula were not covered as the guide can only sit at a specific predefined position (Figure 4.4). During the

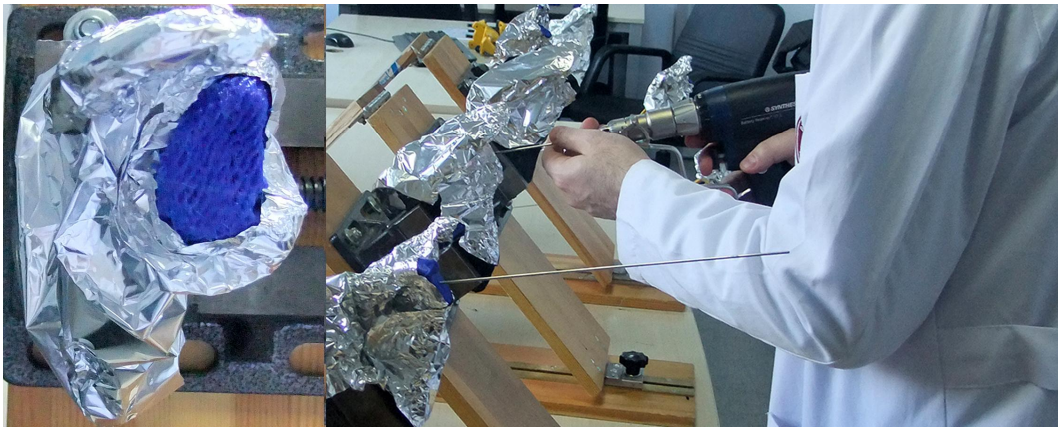

Figure 4.3 : (Left) Scapula model covered by aluminum foil, mounted on the fixture, (Right) Experiment setup, surgeon inserting the guide pin with the freehand method.

Figure 4.4 : (Left) Inserting guide pin using a general guide, (Center and Right) ShoulderART PSI guide mounted on the glenoid.

experiment, all models were recoded to be distinguished based on the surgeon and the method.

4.3 Measurement Method

To observe the results of the experiment, post-operative CT scans of the models and guide pins were obtained using the same CT scan protocol used for capturing initial images to be used with the software. Next, these CT images were used to create 3D models of the bones with the guide pin in place inside the bone.

The 3D models of each sample were registered in 3D space to match each other exactly (Figure 4.5). Then, using the Friedman and Maurer methods, the version and inclination of the 3D models were measured digitally. The position of the guide pin entrance to the glenoid surface was also measured in reference to the planned entry

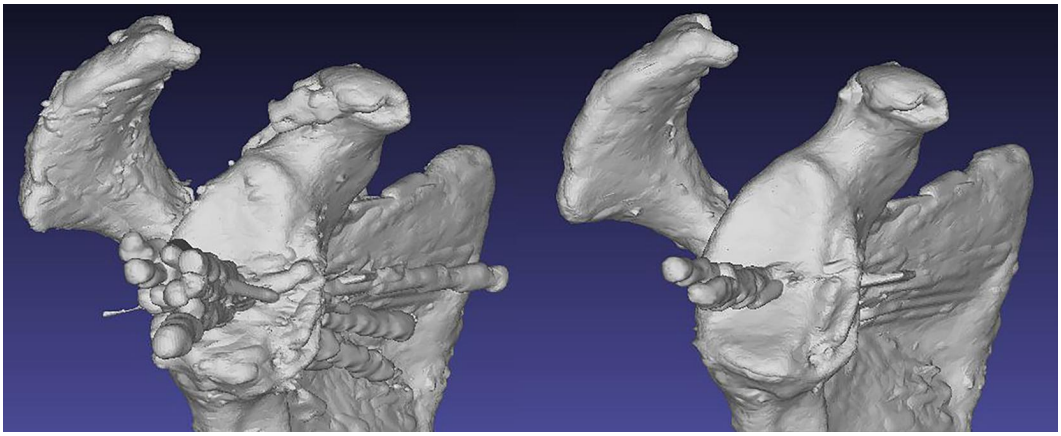

Figure 4.5 : 3D models of each sample registered in 3D space, Left) The freehand method, Right) PSI method.

point. The mean value and standard deviation of the version, and inclination and entry point locations were measured for each sample operated on by each method.

The measurement results were used for two types of evaluation. First, the reliability and precision of the patient-specific guide in positioning the guide pin on different glenoid types were assessed. Second, the PSI method was compared to the other two conventional methods.

For the evaluation of reliability and precision, the actual experimental results were compared to the values decided in the preoperative planning.

When comparing the PSI method to the other methods, the results were evaluated to determine if the patient-specific guide had advantages over conventional methods.

The version and inclination angle errors were defined as the absolute values of the differences between the planned and postoperative angles. The error for the entry point offset was defined as the absolute value of the distance of the post-operative entry point in reference to the planned entry point.

IBM SPSS Statistics for Windows, version 24.0 was used to conduct all statistical analyses. Analysis of variance (ANOVA) and two-way ANOVA were employed for all comparisons. Duncan's post-hoc tests were used to differentiate the subgroups. A significance level of 0.05 was used to determine statistically significant results. For the sample size of 50 for each group, assuming ANOVA at a significance level of 0.05, a power calculation of 0.78 was obtained for the experiment.

5. RESULTS

The first purpose of the experiment of this study was to evaluate the ability of the software tool to provide proper preoperative planning service to the surgeon and then create proper guides for the specific patients. The next purpose of the experiment was to evaluate the accuracy of the results of the operations performed when preoperative planning is done by this software for different glenoid types.

The experiment shows that for all the cases used, all sections of the software could work without any issues and the software could present the required information to the user and the user could finalize the desired PSI guide using the software. The software was able to create and save the PSI guide based on the patient's anatomy and the designed guide could be physically manufactured and be used on the patient's bone. The use of landmark points by the guide could correctly create a fixed positioning on the glenoid surface and the seating of the guide on the glenoid surface was recognized to be smooth and firm. Accordingly, it is observed that the software tool results can positively satisfy the first aim of the experiment.

To be able to evaluate the software from the point of view of the second purpose of the experiment and analyze the accuracy of the operation performed using the created guide the following results are found.

The values of the glenoid version and glenoid inclination angles are shown in Tables 5.1 and 5.2. The values of version and inclination angle deviation from the plan are presented once for all types and once for each type of scapula separately (Table 5.3).

When all types were considered collectively, the deviation of the overall version angle from the plan was $2.68 \pm 2.10^{\circ}$, the overall inclination angle deviation from the plan was $2.59 \pm 2.68^{\circ}$, and the deviation of the entry point offset from the plan was 1.55 ± 1.26 mm.

Table 5.1 : The real values of the glenoid native version angle, planned version angle, and post-operative achieved version angle for each type of scapula only for the PSI method.

Group	Native version *(deg)*	Planned version *(deg)*	Post-Operative version	
			Mean *(deg)*	SD *(deg)*
Non-arthritic	-2.30	7.60	9.07	1.52
A2	0.00	6.90	4.89	1.74
B2	-9.70	4.20	3.95	3.02
C	-2.50	0.00	-1.34	2.89
D	1.50	-3.70	-1.76	4.82

Table 5.2 : The real values of the glenoid native inclination angle, planned inclination angle, and post-operative achieved inclination angle for each type of scapula only for the PSI method.

Group	Native inclination *(deg)*	Planned inclination *(deg)*	Post-Operative inclination	
			Mean *(deg)*	SD *(deg)*
Non-arthritic	87.00	90.60	91.99	1.49
A2	74.00	92.30	90.81	2.35
B2	85.60	100.60	102.27	1.35
C	77.40	86.90	88.29	2.84
D	81.70	99.40	94.65	4.53

The values of deviation from the plan for each method, for all groups collectively, and for each scapula type separately, with their respective P-values for the comparison of the PSI method to the other methods are shown in Table 5.4 .

When all the groups were analyzed together, the PSI method was better than the other methods. The version angle deviation from the plan for PSI $(2.68^\circ \pm 2.10^\circ)$ was significantly better than those of the other methods (conventional guide:$6.44^\circ \pm 4.62^\circ$, freehand:$6.86^\circ \pm 4.43^\circ$, P-value <0.05). The inclination angle deviation from the plan for PSI $(2.59^\circ \pm 2.68^\circ)$ was also significantly better than those of the conventional guide $(6.31^\circ \pm 4.45^\circ)$ and freehand $(7.44^\circ \pm 4.76^\circ)$ (P <0.05). Finally, the entry point offset deviation from the plan for PSI $(1.55mm \pm 1.26mm)$ was also significantly better than those of the other methods (conventional guide:$2.29mm \pm 1.74mm$, freehand:$2.17mm \pm 1.48mm$, P <0.05).

In addition to comparisons of the deviations from the plan values between the three different methods, significant differences were also observed separately between all three methods (Table 5.5).

Table 5.3 : The deviation from the plan (error) values between planned and post-operative version angle, inclination angle, and entry point offset for the PSI method.

Group	Variable	Mean	SD	Min	Max
All groups	Version *(deg)*	2.68	2.10	0.30	8.60
	Inclination *(deg)*	2.59	2.68	0.00	16.90
	Entry point offset *(mm)*	1.55	1.26	0.01	5.21
Non-arthritic	Version *(deg)*	1.89	0.95	0.30	3.20
	Inclination *(deg)*	1.57	1.29	0.30	5.10
	Entry point offset *(mm)*	1.59	0.93	0.22	3.20
A2	Version *(deg)*	2.49	0.93	0.78	3.70
	Inclination *(deg)*	2.07	1.86	0.00	6.30
	Entry point offset *(mm)*	1.91	0.78	0.50	2.83
B2	Version *(deg)*	2.27	2.01	0.30	6.90
	Inclination *(deg)*	1.81	1.15	0.30	4.30
	Entry point offset *(mm)*	1.92	0.72	0.25	2.80
C	Version *(deg)*	2.50	1.98	0.60	6.70
	Inclination *(deg)*	2.65	1.72	0.90	6.80
	Entry point offset *(mm)*	0.06	0.04	0.01	0.15
D	Version *(deg)*	4.26	2.98	0.50	8.60
	Inclination *(deg)*	4.87	4.40	0.60	16.90
	Entry point offset *(mm)*	2.28	1.73	0.32	5.21

Table 5.4 : Version angle, inclination angle, and entry point offset deviation from the plan (error) values, for each method, for all groups collectively and each group separately.

Groups	Method	Version (Mean ± SD) *(deg)*	Inclination (Mean ± SD) *(deg)*	Entry Point Offset (Mean ± SD) *(mm)*
All Groups	Freehand	6.86 ± 4.43	7.44 ± 4.76	2.17 ± 1.48
	Conventional guide	6.44 ± 4.62	6.31 ± 4.45	2.29 ± 1.74
	PSI	2.68 ± 2.10	2.59 ± 2.68	1.55 ± 1.26
	P. Value	0.035	0.000	0.000
Non-arthritic	Freehand	9.8 ± 4.24	9.71 ± 6.16	2.38 ± 0.75
	Conventional guide	9.76 ± 5.29	4.45 ± 3.19	2.84 ± 1.69
	PSI	1.89 ± 0.95	1.57 ± 1.29	1.59 ± 0.93
	P. Value	0.000	0.008	0.100
A2	Freehand	4.16 ± 2.75	6.71 ± 4.0	2.27 ± 0.91
	Conventional guide	4.37 ± 2.35	6.43 ± 3.26	2.18 ± 1.05
	PSI	2.49 ± 0.93	2.07 ± 1.86	1.91 ± 0.78
	P. Value	0.149	0.134	0.689
B2	Freehand	6.59 ± 3.43	6.23 ± 3.99	2.96 ± 1.02
	Conventional guide	5.4 ± 3.46	6.54 ± 5.25	2.99 ± 1.62
	PSI	2.27 ± 2.01	1.81 ± 1.15	1.92 ± 0.72
	P. Value	0.424	0.070	0.107
C	Freehand	9.9 ± 4.29	9.49 ± 3.40	0.10 ± 0.06
	Conventional guide	8.6 ± 5.39	7.47 ± 3.74	0.14 ± 0.05
	PSI	2.5 ± 1.98	2.65 ± 1.72	0.064 ± 0.04
	P. Value	0.001	0.001	0.025
D	Freehand	3.86 ± 2.45	5.06 ± 3.40	3.11 ± 1.55
	Conventional guide	4.09 ± 1.84	6.7 ± 5.18	3.30 ± 1.36
	PSI	4.26 ± 2.98	4.87 ± 4.40	2.28 ± 1.73
	P. Value	0.227	0.298	0.345

The version angle of the PSI method was significantly better than those of the conventional guide and freehand methods (P <0.05). The PSI method was significantly better than the conventional guide method (P <0.05) but was in the same subgroup as the freehand method (P <0.05) for the inclination angle. The PSI method was in the same subgroup as the other methods (P = 0.054) for the entry point offset.

Analysis of the groups separately showed that the PSI method had comparable but not superior results than of the other methods for four of the values; namely, the mean and standard deviation of the version angle, the standard deviation of the inclination angle, and the standard deviation of the entry point offset in the type D group and the standard deviation of the entry point offset in the non-arthritic group.

Except for these four values, the PSI method showed better accuracy than those of the other methods, indicating the advantages of the PSI method.

The version angle deviation from the plan for PSI $(1.89^\circ \pm 0.95^\circ)$ in the non-arthritic group was significantly better than that for the other methods (conventional guide: $9.76^\circ \pm 5.29^\circ$, freehand: $9.8^\circ \pm 4.24^\circ$, P <0.05). The inclination angle deviation from the plan for PSI in the non-arthritic group $(1.57^\circ \pm 1.29^\circ)$ was better than that of the other methods (conventional guide: $4.45^\circ \pm 3.19^\circ$, freehand: $9.71^\circ \pm 6.16^\circ$, P <0.05).

The version angle from the plan for PSI in the type A2 group $(2.49^\circ \pm 0.93^\circ)$ was better than those for the conventional guide$(4.37^\circ \pm 2.35^\circ)$ and freehand $(4.16^\circ \pm 2.75^\circ)$, (P = 0.149) methods. The inclination angle deviation from the plan for PSI in the A2 group $(2.07^\circ \pm 1.86^\circ)$ was better than that for the other methods (conventional guide: $6.43^\circ \pm 3.26^\circ$, freehand: $6.71^\circ \pm 4.0^\circ$, P = 0.134). The entry point offset from the plan for PSI in the A2 group $(1.91.mm \pm 0.78mm)$ was better than those of the conventional guide $(2.18mm \pm 1.05mm)$ and freehand $(2.27mm \pm 0.91mm)$ (P = 0.689).

The version angle deviation from the plan for PSI in the B2 group $(2.27^\circ \pm 2.01^\circ)$ was better than those for the conventional guide $(5.4^\circ \pm 3.46^\circ)$ and freehand $(6.59^\circ \pm 3.43^\circ)$ (P = 0.424). The inclination angle deviation from the plan for PSI in the B2 group $(1.81^\circ \pm 1.15^\circ)$ was better than those for the conventional guide $(6.54^\circ \pm 5.25^\circ)$ and freehand $(6.23^\circ \pm 3.99^\circ)$ (P = 0.07). The entry point offset deviation from the plan for PSI in the B2 group $(1.92.mm \pm 0.72mm)$ was better than those of the other

Table 5.5 : The quantification of the significance of differences observed between all three methods for all groups collectively.

All Groups			
Inclination	Method	Subset	
		1	2
	2	-4.338	
	3		-0.358
	1		1.512
	P. Value	0.033	0.015
Version		1	2
	1	-5.430	
	2	-3.912	
	3		-0.386
	P. Value	0.044	0.031
Entry Point Offset		1	
	3	1.550	
	1	2.160	
	2	2.290	
	P. Value	0.054	

methods (conventional guide: $2.99mm \pm 1.62mm$, freehand: $2.96mm \pm 1.02mm$, P= 0.107).

The version angle deviation from the plan for PSI in the type C group $(2.5^\circ \pm 1.98^\circ)$ was significantly better than those of the other methods (conventional guide: $8.6^\circ \pm 5.39^\circ$, freehand:$9.9^\circ \pm 4.29^\circ$, P-value <0.05). The inclination angle deviation from the plan for PSI in the type C group $(2.65^\circ \pm 1.72^\circ)$ was significantly better than those of the other methods (conventional guide: $7.47^\circ \pm 3.47^\circ$, freehand: $9.49^\circ \pm 3.4^\circ$, P-value <0.05). The entry point offset deviation from the plan for PSI in the type C group $(0.064mm \pm 0.04mm)$ was better than those of the conventional guide $(0.14mm \pm 0.05mm)$ and freehand $(0.10mm \pm 0.05mm)$, (P <0.05).

Since the deviations from the plan values were compared between the three different methods, the differences were also assessed separately between all three methods for the non-arthritic and type C groups (Table 5.6).

For the non-arthritic group, the version angle of the PSI method was significantly better than those for the conventional guide and freehand methods (P <0.05). The PSI method was significantly better than the freehand method (P <0.05) but was in the same subgroup as the conventional guide method (P <0.05) for the inclination angle. The

PSI method was significantly better than the conventional guide method (P = 0.420) but was in the same subgroup as the freehand method (P= 0.174) for the entry point offset.

For the type C group, the PSI method had a significantly better inclination angle than that of the conventional guide method (P <0.05) but was in the same subgroup as the freehand method (P =0.250). The PSI method was significantly better than the conventional guide method (P <0.05) but was in the same subgroup as the freehand method for entry point offset (P <0.05). The PSI method was significantly better than the other two methods for the version angle (P <0.05).

No statistically significant differences were observed between the two surgeons in terms of the deviation from the plan for version angle, inclination angle, and entry point offset.

Table 5.6 : The quantification of the significance of differences observed between all three methods for each group.

	Non-arthritic Group			Group A2		Group B2			Group C			Group D	
		Subset			Subset		Subset			Subset			Subset
Inclination	Method	1	2	Method	1	Method	1	2	Method	1	2	Method	1
	3	1.390		2	-6.050	2	-6.520		2	-5.150		2	-6.620
	2	2.650		1	-1.910	1	-3.370		3		1.390	3	-4.750
	1		8.990	3	-1.490	3		1.670	1		6.650	1	-2.800
	P. Value	0.033	0.012		0.085		0.015	0.022		0.044	0.250		0.143
Version		1	2		1		1			1	2		1
	1	-9.800		2	-4.370	1	-2.930		1	-9.900		1	-0.800
	2	-9.760		1	-3.720	3	-0.250		2	-8.500		3	1.940
	3		1.470	3	-2.013	2	0.440		3		-1.340	2	2.630
	P. Value	0.044	0.031		0.074		0.245			0.030	0.025		0.125
Entry Point Offset		1	2		1		1			1	2		1
	3	1.590		3	1.912	3	1.914		3	0.064		3	2.278
	1	2.376	2.376	2	2.186	1	2.964		1	0.101	0.101	1	3.111
	2		2.837	1	2.273	2	2.987		2		0.135	2	3.305
	P. Value	0.174	0.420		0.44		0.078			0.040	0.043		0.197

6. DISCUSSION

In this work, a 3D preoperative planning software for shoulder arthroplasty was developed using open source libraries. To develop such a software tool the medical condition has been investigated first, and then the type and properties of the input data as CT scan images have been studied. Next, the operations to be performed on the input data to reach the final software are devised, and the general process of the preoperative planning is planned. Using the general process, each step of the process is designed and developed. For each step, required algorithms and software tools are found, developed, and integrated.

For capturing, reading the input data, importing it to the software environment, sorting and saving the data, different protocols and standards are used. A specific CT scan protocol is selected for the software that provides the best data capturing method to be used in the following steps. DICOM standard, GDCM, and VTK libraries are then used for handling the captured data. Internationally accepted fields and details of the DICOM standard makes the data handling very efficient and using the GDCM and VTK libraries makes the data accessing smooth.

For preprocessing the captured and sorted data, contrast stretching and noise removal processes are performed. Particular noise removal algorithms that can preserve the important information in the data are chosen and their implementation in the ITK library is used that makes the process very reliable.

For detection of the bones from all tissues and then detecting scapula bone and its features, new algorithms and methods are developed and VTK library is used. For separating bones from other tissues new algorithm is developed to use the specifically selected CT scan protocol and patient data for automatic threshold detection of each patient. For detecting the scapula bone from other bones the geometrical properties of the bones in the shoulder area are considered to conceive a bone separation method. To detect features of the scapula bone, many different geometrical properties, the general shape of the scapula bone and glenoid surface, and a combination of point and surface

detection algorithms are used. Parts of algorithms use VTK library and some parts are developed solely using C++ language where libraries do not meet the specific requirements of the problem at hand.

The design of the GUI of the software and software-assisted preoperative planning are performed together. The GUI sections' layout and available features are designed having in mind their functionality for the preoperative planning. The GUI uses VTK and Qt libraries for rendering and interface design. The preoperative planning process is designed both taking into consideration the technical aspects of the software and the feedback from the surgeons as the user of the software. For designing the guide VTK, CGAL, and OpenMesh libraries are used. The algorithms and the geometric shape of the guide are designed in such a way that the process can be fully automatic for each specific patient, and the guide has proper seating on the glenoid and good mechanical strength for the drilling operation.

Methods and algorithms developed in this work are designed to be optimized for solving the tasks at each section of the software. The libraries used are all considered to be well established and well known open source libraries that can be accessed by other developers. All these algorithms and libraries provide the possibility to create a patient specific guide for each medical case. These cases then can be used to test the developed software.

An experiment was designed and performed on 3D patient-specific guides created by 3D preoperative planning. The aim of the experiment was twofold, firstly to observe the ability of the software tool to provide proper preoperative planning service to the surgeon and create proper guides for the specific patients. And secondly, to evaluate the accuracy and reliability of the PSI for guide pin positioning as well as for the comparison of the PSI method to conventional methods.

The experiment showed that for all cases the software was capable of creating proper PSI guides. The preoperative planning performed using the software by the surgeons was a successful experience and the surgeons were satisfied with the guides created. As a result the functionality of the algorithms used in the software were approved to be working in accordance with the aims of the software development.

The results of the experiment were also evaluated for the analysis of the second aim of the experiment. The accuracy and reliability of the PSI were tested by comparing the version angle, inclination angle, and entry point offset between the actual post-operative results and the planned values using the PSI method.

As shown in Tables 5.1 , 5.2 , and 5.3 , the post-operative values of the PSI method were very close to the planned values and the patient-specific guide achieved the planned values with good accuracy.

The results were also evaluated for the comparison of the PSI method to conventional methods. As shown in Tables 5.4 , 5.5 , and 5.6 , when all types are considered together, the error values of the PSI method showed better mean and standard deviation than those of the other methods.

Comparisons of error values between different types showed better mean and standard deviation values for the PSI for all groups, except for four values, with significant differences in the non-arthritic and type C groups. The exceptions were the mean and standard deviation of the version angle, the standard deviation of the inclination angle, and the standard deviation of the entry point offset in the type D group and the standard deviation of the entry point offset in the non-arthritic group.

The standard deviation of the data for different glenoid types and how a patient-specific guide reduced the chance of extreme malpositioning are shown in Figure 6.1.While the PSI guide showed mean version and inclination angle values and standard deviations very close to the planned values, the mean values of the other methods did not always agree with the planned values. This observation demonstrates how surgeons can make different decisions about implant positioning when they are provided more visual information about the scapula. These results showed that patient-specific guides can help to reduce the risks of surgery complications resulting from deciding the wrong positioning of the guide pin without sufficient visual preoperative data.

Other studies have also shown the accuracy of using patient-specific guides in shoulder arthroplasty. Levy et al. [13] reported a translational accuracy of $1.2 \pm 0.7mm$, inferior tilt accuracy of $1.2^\circ \pm 1.2^\circ$, and glenoid version accuracy of $2.6^\circ \pm 1.7^\circ$ in their evaluation of the accuracy of patient-specific planning and a patient-specific drill guide for glenoid baseplate placement in RSA. Walch et al. [17] showed a mean entry point

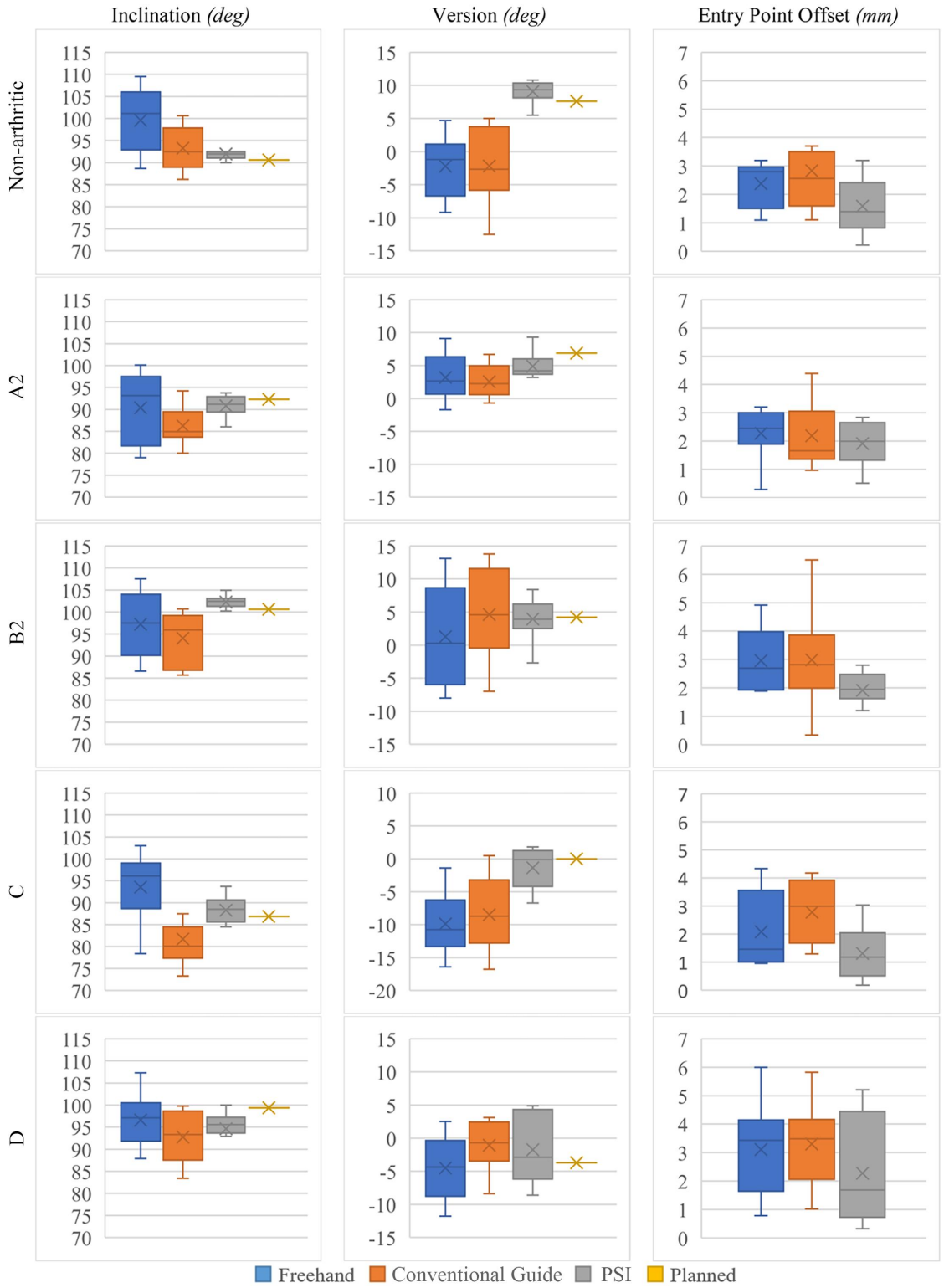

Figure 6.1 : Comparison of results of three different methods for each group's version angle, inclination angle, and guide pin entry point distance.

position error of 1.05 mm, a mean inclination angle error of 1.42, and an average error in the version angle of 1.64°. In our study, the entry point offset accuracy was $1.55mm \pm 1.26mm$, the inclination angle accuracy was $2.59° \pm 2.68°$, and the version angle accuracy was$2.68° \pm 2.10°$ for all samples.

This study evaluated the accuracy of the PSI method in guide pin positioning and found that PSI was more beneficial than conventional guide and freehand instrumentation methods in cases with glenoid bone deformity. The results of this study demonstrated that the developed software is capable of performing the desired tasks in preoperative planning and guide design operations. It also validated the guide pin positioning accuracy of PSI and showed that, for non-arthritic glenoid type and defective glenoid types C, B2, and A2, PSI was more accurate than other methods, although the results were statistically meaningful for non-arthritic glenoid and defective glenoid type C.

7. CONCLUSION

This thesis work started by observing a problem in shoulder arthroplasty operations. Complications that occur in RSA affect the success rate of the operation and the longevity inserted prosthesis. These issues gave the team the purpose to find a solution. Loosening of the glenoid component, one of the major complications in RSA, which is caused mainly by incorrect positioning, is aimed to be improved. The correct glenoid component positioning is difficult to achieve manually and hence a hypothesis of this work was to use patient specific instrumentation technology to create a guiding system to help the accuracy of the positioning. The goal was to create a guiding system that can improve the positioning and test to observe the functioning of such a guide for different patients. To reach this goal multiple methods are elaborated, multiple tools are explored, and different algorithms are developed. Patient specific instrumentation technology is researched so that the guiding system can meet the specific needs of each patient and the specific anatomy of each shoulder joint. On the road to apply patient specific instrumentation, pre-operative planning is found a necessary step. With proper pre-operative planning and evaluation of the specific conditions of each case is that the surgeon can decide the best PSI guide, and pre-operative planning itself relies on a good software application that can provide relative and necessary information to the surgeon through its graphical user interface. As a result, a software tool is developed to support PSI guide creation, pre-operative planning, and a graphical user interface.

For developing the software to create a PSI guide, several steps are carried out. Interfacing and sorting the input data, preprocessing the imported images, detection of the bones from other tissues in the images, detection of certain features from the scapula bone, and creating a guide to fit the glenoid surface of the scapula bone are the processes that had to be achieved so that the PSI system could work. For each of these processes, various software libraries are investigated and integrated into the main software, and various algorithms are defined and tested to solve each specific part of the work.

For the software to provide the surgeon with pre-operative planning capability and a proper GUI, the planning process steps required from the medical perspective are decided in the team and the software algorithms and libraries to support them are created and implemented. The design of The GUI and layouts of the sections of the software are created to support the tools required for pre-operative planning steps. For designing and coding the GUI of the software additional software libraries are tested and implemented.

The software then is tested to figure out the accuracy of the guide system and to check the functionality of the developed solution. Accordingly, an experiment is designed and the requirements to perform the experiment is decided. The software is used by surgeons to create guides for certain patients with different glenoid conditions and then the experiment materials and tools are manufactured or prepared. The team has performed the experiment and the results of the experiment are measured, analyzed, and evaluated from different perspectives, to answer the hypothesis of the study.

One hypothesis of this work was that an open-source software platform can be developed that can facilitate preoperative planning abilities and PSI guide creations with high accuracy compared to other non PSI methods of shoulder arthroplasty operations. Where the results were evaluated for the comparison of the PSI method to conventional methods, the error values of the PSI method showed better mean and standard deviation than those of the other methods as explained in detail in the discussion section.

Another hypothesis of this work was that PSIs designed using preoperative planning software would provide better guide pin positioning than standard guided and freehand instrumentation methods, especially in cases of glenoid bone deformity. It is observed that error values of different types of glenoids showed better mean and standard deviation values for the PSI for most of the glenoid groups as described in detail in the discussion section.

Overall the study results support the initial aims and hypotheses it was trying to prove and reach and the created tool developed using only open-source libraries can be a blueprint for further researches.

7.1 Limitations and Further Work

This study had some limitations. Although 30 samples from every five types of scapula were tested, future research should test more glenoid types to further evaluate the accuracy and performance of the method. In this respect, more experiments can be performed including new specimens and new patients.

Another limitation of this study was that the scapula models used for the experiment did not have any soft tissue coverage on the glenoid surface as would be present in actual surgical interventions. To eliminate this issue future experiments can be performed using cadaveric models.

In succeeding studies the current software can be improved to be enabled for performing preoperative planning on orthopedics surgeries on other joints of the body and other types of surgeries. Different guide designs can be investigated based on the needs of the specific body parts. Surgeries performed on the elbow can be the first example in this list where the existing software can be improved be applied.

The current software can benefit from virtual reality technology. Using this technology the surgeon can see the anatomy of the patient and perform all the current preoperative planning steps in three-dimensional virtual space. The combination of the current study with the augmented reality technology is another feature that can be very advantageous.

Using augmented reality the three-dimensional model of the bones of the patient that are extracted and showed on the software will be projected on the real body of the patient through special glasses that the surgeon wears. This way the surgeon can more clearly evaluate all the aspects of the operation and the design of the guide model based on the extra information that can be perceived from the body.

Applying machine learning techniques can also improve this study in different sections. Having enough number of medical cases to use as the data, the design of the guide and sections of the algorithms used can be improved by machine learning.

REFERENCES

[1] **Deutsch, A.**, **Abboud, J.A.**, **Kelly, J.**, **Mody, M.**, **Norris, T.**, **Ramsey, M.L. ... Williams, G.R.** (2007). Clinical results of revision shoulder arthroplasty for glenoid component loosening, *Journal of Shoulder and Elbow Surgery*, *16*(6), 706–716.

[2] **Walch, G.**, **Boileau, P. and Noël, E.** (2010). Shoulder arthroplasty: Evolving techniques and indications, *Joint Bone Spine*, *77*(6), 501–505, `http://dx.doi.org/10.1016/j.jbspin.2010.09.004`.

[3] **Zumstein, M.A.**, **Pinedo, M.**, **Old, J. and Boileau, P.** (2011). Problems, complications, reoperations, and revisions in reverse total shoulder arthroplasty: a systematic review., *Journal of shoulder and elbow surgery*, *20*(1), 146–157.

[4] **Hasan, S.S.**, **Leith, J.M.**, **Campbell, B.**, **Kapil, R.**, **Smith, K.L. and Matsen, F.A.** (2002). Characteristics of unsatisfactory shoulder arthroplasties, *Journal of Shoulder and Elbow Surgery*, *11*(5), 431–441.

[5] **Hoenecke, H.R.**, **Hermida, J.C.**, **Dembitsky, N.**, **Patil, S. and D'Lima, D.D.** (2008). Optimizing glenoid component position using three-dimensional computed tomography reconstruction, *Journal of Shoulder and Elbow Surgery*, *17*(4), 637–641.

[6] **Codsi, M.J. and Iannotti, J.P.** (2008). The effect of screw position on the initial fixation of a reverse total shoulder prosthesis in a glenoid with a cavitary bone defect, *Journal of Shoulder and Elbow Surgery*, *17*(3), 479–486.

[7] **Lobao, M.H. and Murthi, A.M.** (2018). Pitfalls of revision reverse replacement part I: dealing with instability and glenoid bone loss, *Annals of Joint*, *3*(3), 99–99.

[8] **Nguyen, D.**, **Ferreira, L.M.**, **Brownhill, J.R.**, **King, G.J.W.**, **Drosdowech, D.S. ... Johnson, J.A.** (2009). Improved accuracy of computer assisted glenoid implantation in total shoulder arthroplasty: An in-vitro randomized controlled trial, *Journal of Shoulder and Elbow Surgery*, *18*(6), 907–914, `http://dx.doi.org/10.1016/j.jse.2009.02.022`.

[9] **Iannotti, J.P.**, **Greeson, C.**, **Downing, D.**, **Sabesan, V. and Bryan, J.A.** (2012). Effect of glenoid deformity on glenoid component placement in primary shoulder arthroplasty, *Journal of Shoulder and Elbow Surgery*, *21*(1), 48–55, `http://dx.doi.org/10.1016/j.jse.2011.02.011`.

[10] **Karelse, A.**, **Leuridan, S.**, **Van Tongel, A.**, **Piepers, I.M.**, **Debeer, P. and De Wilde, L.F.** (2014). A glenoid reaming study: How accurate are current reaming techniques?, *Journal of Shoulder and Elbow Surgery*, *23*(8), 1120–1127, http://dx.doi.org/10.1016/j.jse.2013.11.023.

[11] **Ackland, D.C.**, **Patel, M. and Knox, D.** (2015). Prosthesis design and placement in reverse total shoulder arthroplasty, *Journal of Orthopaedic Surgery and Research*, *10*(1), 1–9, http://dx.doi.org/10.1186/s13018-015-0244-2.

[12] **Burns, D.M.**, **Frank, T.**, **Whyne, C.M. and Henry, P.D.** (2019). Glenoid component positioning and guidance techniques in anatomic and reverse total shoulder arthroplasty: A systematic review and meta-analysis, *Shoulder and Elbow*, *11*(2_suppl), 16–28.

[13] **Levy, J.C.**, **Everding, N.G.**, **Frankle, M.A. and Keppler, L.J.** (2014). Accuracy of patient-specific guided glenoid baseplate positioning for reverse shoulder arthroplasty, *Journal of Shoulder and Elbow Surgery*, *23*(10), 1563–1567, https://linkinghub.elsevier.com/retrieve/pii/S1058274614000962.

[14] **Hendel, M.D.**, **Bryan, J.A.**, **Barsoum, W.K.**, **Rodriguez, E.J.**, **Brems, J.J.**, **Evans, P.J. and Iannotti, J.P.** (2012). Comparison of Patient-Specific Instruments with Standard Surgical Instruments in Determining Glenoid Component Position, *The Journal of Bone and Joint Surgery-American Volume*, *94*(23), 2167–2175, https://insights.ovid.com/crossref?an=00004623-201212050-00010.

[15] **Iannotti, J.**, **Baker, J.**, **Rodriguez, E.**, **Brems, J.**, **Ricchetti, E.**, **Mesiha, M. and Bryan, J.** (2014). Three-Dimensional Preoperative Planning Software and a Novel Information Transfer Technology Improve Glenoid Component Positioning, *The Journal of Bone and Joint Surgery-American Volume*, *96*(9), e71–1–8, https://insights.ovid.com/crossref?an=00004623-201405070-00006.

[16] **Suero, E.M.**, **Citak, M.**, **Lo, D.**, **Krych, A.J.**, **Craig, E.V. and Pearle, A.D.** (2013). Use of a custom alignment guide to improve glenoid component position in total shoulder arthroplasty, *Knee Surgery, Sports Traumatology, Arthroscopy*, *21*(12), 2860–2866, http://link.springer.com/10.1007/s00167-012-2177-1.

[17] **Walch, G.**, **Vezeridis, P.S.**, **Boileau, P.**, **Deransart, P. and Chaoui, J.** (2015). Three-dimensional planning and use of patient-specific guides improve glenoid component position: an in vitro study, *Journal of Shoulder and Elbow Surgery*, *24*(2), 302–309, https://linkinghub.elsevier.com/retrieve/pii/S1058274614003280.

[18] **Scalise, J.J.**, **Bryan, J.**, **Polster, J.**, **Brems, J.J. and Iannotti, J.P.** (2008). Quantitative analysis of glenoid bone loss in osteoarthritis using three-dimensional computed tomography scans, *Journal of Shoulder*

and Elbow Surgery, *17*(2), 328–335, https://linkinghub.elsevier.com/retrieve/pii/S1058274607006209.

[19] **Hoenecke, H.R.**, **Hermida, J.C.**, **Flores-Hernandez, C. and D'Lima, D.D.** (2010). Accuracy of CT-based measurements of glenoid version for total shoulder arthroplasty, *Journal of Shoulder and Elbow Surgery*, *19*(2), 166–171, https://linkinghub.elsevier.com/retrieve/pii/S105827460900425X.

[20] **Scalise, J.J.**, **Codsi, M.J.**, **Bryan, J.**, **Brems, J.J. and Iannotti, J.P.** (2008). The Influence of Three-Dimensional Computed Tomography Images of the Shoulder in Preoperative Planning for Total Shoulder Arthroplasty, *The Journal of Bone and Joint Surgery-American Volume*, *90*(11), 2438–2445, https://insights.ovid.com/crossref?an=00004623-200811000-00015.

[21] **Ganapathi, A.**, **McCarron, J.A.**, **Chen, X. and Iannotti, J.P.** (2011). Predicting normal glenoid version from the pathologic scapula: a comparison of 4 methods in 2- and 3-dimensional models, *Journal of Shoulder and Elbow Surgery*, *20*(2), 234–244, https://linkinghub.elsevier.com/retrieve/pii/S1058274610002429.

[22] **Berhouet, J.**, **Gulotta, L.V.**, **Dines, D.M.**, **Craig, E.**, **Warren, R.F.**, **Choi, D.**, **Chen, X. and Kontaxis, A.** (2017). Preoperative planning for accurate glenoid component positioning in reverse shoulder arthroplasty, *Orthopaedics and Traumatology: Surgery and Research*, *103*(3), 407–413, http://dx.doi.org/10.1016/j.otsr.2016.12.019.

[23] **Heylen, S.**, **Van Haver, A.**, **Vuylsteke, K.**, **Declercq, G. and Verborgt, O.** (2016). Patient-specific instrument guidance of glenoid component implantation reduces inclination variability in total and reverse shoulder arthroplasty, *Journal of Shoulder and Elbow Surgery*, *25*(2), 186–192, https://linkinghub.elsevier.com/retrieve/pii/S105827461500405X.

[24] **Lewis, G.S.**, **Stevens, N.M. and Armstrong, A.D.** (2015). Testing of a novel pin array guide for accurate three-dimensional glenoid component positioning, *Journal of Shoulder and Elbow Surgery*, *24*(12), 1939–1947, https://linkinghub.elsevier.com/retrieve/pii/S1058274615003420.

[25] **Throckmorton, T.W.**, **Gulotta, L.V.**, **Bonnarens, F.O.**, **Wright, S.A.**, **Hartzell, J.L.**, **Rozzi, W.B. ... Sperling, J.W.** (2015). Patient-specific targeting guides compared with traditional instrumentation for glenoid component placement in shoulder arthroplasty: a multi-surgeon study in 70 arthritic cadaver specimens, *Journal of Shoulder and Elbow Surgery*, *24*(6), 965–971, https://linkinghub.elsevier.com/retrieve/pii/S1058274614005795.

[26] **Walch, G.**, **Boulahia, A.**, **Boileau, P. and Kempf, J.F.** (1998). Primary glenohumeral osteoarthritis: clinical and radiographic classification. The

Aequalis Group., *Acta orthopaedica Belgica*, *64 Suppl 2*, 46–52, http://www.ncbi.nlm.nih.gov/pubmed/9922529.

[27] **Lévigne, C.**, **Boileau, P.**, **Favard, L.**, **Garaud, P.**, **Molé, D.**, **Sirveaux, F. and Walch, G.** (2008). Scapular notching in reverse shoulder arthroplasty, *Journal of Shoulder and Elbow Surgery*, *17*(6), 925–935.

[28] **Friedman, R.J.**, **Hawthorne, K.B. and Genez, B.M.** (1992). The use of computerized tomography in the measurement of glenoid version., *The Journal of Bone & Joint Surgery*, *74*(7), 1032–1037, http://insights.ovid.com/crossref?an=00004623-199274070-00009.

[29] **Maurer, A.**, **Fucentese, S.F.**, **Pfirrmann, C.W.**, **Wirth, S.H.**, **Djahangiri, A.**, **Jost, B. and Gerber, C.** (2012). Assessment of glenoid inclination on routine clinical radiographs and computed tomography examinations of the shoulder, *Journal of Shoulder and Elbow Surgery*, *21*(8), 1096–1103, http://dx.doi.org/10.1016/j.jse.2011.07.010https://linkinghub.elsevier.com/retrieve/pii/S1058274611003065.

[30] **Clouthier, A.L.**, **Hetzler, M.**, **Fedorak, G.**, **Bryant, J.**, **Deluzio, K. and Bicknell, R.** (2013). Factors affecting the stability of reverse shoulder arthroplasty: a biomechanical study., *Journal of shoulder and elbow surgery*, *22 4*, 439–44.

[31] **Deserno, T.M.** (2011). *Biomedical Image Processing*, Springer-Verlag Berlin Heidelberg.

[32] **Mustra, M.**, **Delac, K. and Grgic, M.** (2008). Overview of the DICOM standard, *2008 50th International Symposium ELMAR*, *1*(September), 39–44.

[33] **Mildenberger, P.**, **Eichelberg, M. and Martin, E.** (2002). Introduction to the DICOM standard, *European Radiology*, *12*(4), 920–927.

[34] **Mathieu Malaterre and al.**, Grassroots DICOM, http://gdcm.sourceforge.net.

[35] **Schroeder, W.**, **Martin, K. and Lorensen, B.**, (2002), Kitware Inc. - The Visualization Toolkit. An Object Oriented Approach to 3D Graphics, 3rd Edition.

[36] **Mccormick, M.**, **Liu, X.**, **Jomier, J.**, **Marion, C. and Ibanez, L.** (2014). Itk: Enabling reproducible research and open science, *Frontiers in Neuroinformatics*, *8*(FEB), 1–11.

[37] Qt, https://www.qt.io/, date accessed: 29.06.2020.

[38] **Board, C.E.**, Computational Geometry Algorithms Library, https://www.cgal.org/.

[39] **University, R.A.**, **and Multimedia, D.o.C.G.**, OpenMesh, www.openmesh.org.

[40] **Gravel, P.**, **Beaudoin, G. and De Guise, J.A.** (2004). A method for modeling noise in medical images, *IEEE Transactions on Medical Imaging*, *23*(10), 1221–1232.

[41] **Bhonsle, D.**, **Chandra, V. and Sinha, G.** (2012). Medical Image Denoising Using Bilateral Filter, *International Journal of Image, Graphics and Signal Processing*, *4*(6), 36–43.

[42] **Lal, S.**, **Chandra, M. and Upadhyay, G.K.** (2011). Removal of Additive Gaussian Noise by Complex Double Density Dual Tree Discrete Wavelet Transform, *1*(1), 8–16.

[43] **Nowak, R.D.** (1999). Wavelet-based Rician noise removal for magnetic resonance imaging, *IEEE Transactions on Image Processing*, *8*(10), 1408–1419.

[44] **Tomasi, C. and Manduchi, R.** (1988). Bilateral filtering for gray and color images, *Sixth International Conference on Computer Vision (IEEE Cat. No.98CH36271)*, 839–846, `http://ieeexplore.ieee.org/document/710815/`.

[45] **Winnemöller, H.**, **Olsen, S.C. and Gooch, B.** (2006). Real-time video abstraction, *ACM SIGGRAPH 2006 Papers on - SIGGRAPH '06*, 1221, `http://portal.acm.org/citation.cfm?doid=1179352.1142018`.

[46] **Bae, S.**, **Paris, S. and Durand, F.** (2006). Two-scale tone management for photographic look, *ACM Transactions on Graphics*, *25*(3), 637, `http://portal.acm.org/citation.cfm?doid=1141911.1141935`.

[47] **Dorsey, J. and Durand, F.** (2002). Fast Bilateral Filtering for the Display of High-Dynamic-Range Images Introduction, *Vine*, 257–266.

[48] **Buades, A.**, **Coll, B. and Morel, J.M.J.M.** (2005). A non-local algorithm for image denoising, *Computer Vision and Pattern Recognition, 2005. CVPR 2005. IEEE Computer Society Conference on*, *2*(0), 60–65 vol. 2.

[49] **Perona, P. and Malik, J.** (1990). Scale-space and edge detection using anisotropic diffusion, *IEEE Transactions on Pattern Analysis and Machine Intelligence*, *12*(7), 629–639, `http://ieeexplore.ieee.org/document/56205/`.

[50] **Barash, D.** (2001). Bilateral filtering and anisotropic diffusion: Towards a unified viewpoint, *Lecture Notes in Computer Science (including subseries Lecture Notes in Artificial Intelligence and Lecture Notes in Bioinformatics)*, *2106*, 273–280.

[51] **Munteanu, C. and Lazarescu, V.** Evolutionary contrast stretching and detail enhancement of satellite images, 3–8.

[52] **Yang, C.C.** (2006). Image enhancement by modified contrast-stretching manipulation, *Optics and Laser Technology*, *38*(3), 196–201.

[53] **Egmentation, S., Pham, D.L., Xu, C. and Prince, J.L.** (2000). Current methods in medical image segmentation, *Annual Review of Biomedical Engineering*, *Vol. 2*, 315–337, https://doi.org/10.1146/annurev.bioeng.2.1.315.

[54] **Sezgin, M. and Sankur, B.** (2004). Survey over image thresholding techniques and quantitative performance evaluation, *Journal of Electronic Imaging*, *13*(1), 146–165, http://electronicimaging.spiedigitallibrary.org/article.aspx?doi=10.1117/1.1631316.

[55] **Fan, J., Yau, D.K.Y., Elmagarmid, a.K. and Aref, W.G.** (2001). Automatic image segmentation by integrating color-edge extractionand seeded region growing, *IEEE Transactions on Image Processing*, *10*(10), 1454–1466.

[56] **Kamavisdar, P., Saluja, S. and Agrawal, S.** (2013). A survey on image classification approaches and techniques, *International Journal of Advanced ...*, *2*(1), 1005–1009, http://ijarcce.com/upload/january/22-ASurveyonImageClassification.pdf.

[57] **Liu, Y., Zhang, D., Lu, G. and Ma, W.Y.** (2007). A survey of content-based image retrieval with high-level semantics, *Pattern Recognition*, *40*(1), 262–282.

[58] **Hegadi, R., Kop, A. and Hangarge, M.** (2010). A Survey on Deformable Model and its Applications to Medical Imaging, *International Journal of Computer Applications*, *RTIPPR*(2), 64–75, http://www.ijcaonline.org/rtippr/number2/SPE101T.pdf{\%}5Cnhttp://files/394/ASurveyonDeformableModelanditsApplications.pdf{\%}5Cnhttp://files/396/SPE101T.html.

[59] **Johnson, C.R. and Tricoche, X.** (2009). *Biomedical Visualization*, Elsevier, first edit edition, http://dx.doi.org/10.1016/B978-0-444-53075-2.00006-X.

[60] **Newman, T.S. and Yi, H.** (2006). A survey of the marching cubes algorithm, *Computers and Graphics (Pergamon)*, *30*(5), 854–879.

[61] **Moineau, G., Levigne, C., Boileau, P., Young, A. and Walch, G.** (2012). Three-dimensional measurement method of arthritic glenoid cavity morphology: Feasibility and reproducibility, *Orthopaedics & Traumatology: Surgery & Research*, *98*(6), S139–S145, http://dx.doi.org/10.1016/j.otsr.2012.06.007https://linkinghub.elsevier.com/retrieve/pii/S1877056812001338.

[62] **Pietrzak, W.S., Pspg, T. and Pspg, T.** (2013). Shoulder Alignment Obtained with the Signature Glenoid Guide System :, (January).

[63] **Iannotti, J.P., Weiner, S., Rodriguez, E., Subhas, N., Patterson, T.E., Jun, B.J. and Ricchetti, E.T.** (2015). Three-dimensional imaging and templating improve glenoid implant positioning, *Journal of Bone and Joint Surgery - American Volume*, *97*(8), 651–658.

[64] **Cabarcas, B.C.**, **Cvetanovich, G.L.**, **Espinoza Orías, A.A.**, **Inoue, N.**, **Gowd, A.K.**, **Bernardoni, E. and Verma, N.N.** (2019). Novel 3-dimensionally printed patient-specific guide improves accuracy compared with standard total shoulder arthroplasty guide: a cadaveric study, *JSES Open Access*, *3*(2), 83–92, https://doi.org/10.1016/j.jses.2019.04.001.

[65] **Theopold, J.**, **Pieroh, P.**, **Scharge, M.L.**, **Marquaß, B.**, **Hohmann, T.**, **Josten, C. and Hepp, P.** (2016). Improved accuracy of K-wire positioning into the glenoid vault by intraoperative 3D image intensifier-based navigation for the glenoid component in shoulder arthroplasty, *Orthopaedics and Traumatology: Surgery and Research*, *102*(5), 575–581, http://dx.doi.org/10.1016/j.otsr.2016.03.013.

[66] **Berhouet, J.**, **Slimane, M.**, **Facomprez, M.**, **Jiang, M. and Favard, L.** (2019). Views on a new surgical assistance method for implanting the glenoid component during total shoulder arthroplasty. Part 2: From three-dimensional reconstruction to augmented reality: Feasibility study, *Orthopaedics and Traumatology: Surgery and Research*, *105*(2), 211–218, https://doi.org/10.1016/j.otsr.2018.08.021.

[67] **Gregory, T.M.**, **Gregory, J.**, **Sledge, J.**, **Allard, R. and Mir, O.** (2018). Surgery guided by mixed reality: presentation of a proof of concept, *Acta Orthopaedica*, *89*(5), 480–483.

[68] **Khan, S.**, **Warkhedkar, R. and Shyam, A.** (2014). Analysis of Hounsfield Unit of Human Bones for Strength Evaluation, *Procedia Materials Science*, *6*(2006), 512–519, http://dx.doi.org/10.1016/j.mspro.2014.07.065.

[69] **Schreiber, J.J.**, **Anderson, P.A. and Hsu, W.K.** (2014). Use of computed tomography for assessing bone mineral density, *Neurosurgical Focus*, *37*(1), 1–8.

[70] **Jagannathan, A. and Miller, E.L.** (2007). Three-dimensional surface mesh segmentation using curvedness-based region growing approach, *IEEE Transactions on Pattern Analysis and Machine Intelligence*, *29*(12), 2195–2204.

[71] **Ghafurian, S.**, **Galdi, B.**, **Bastian, S.**, **Tan, V. and Li, K.** (2016). Computerized 3D morphological analysis of glenoid orientation, *Journal of Orthopaedic Research*, *34*(4), 692–698, http://doi.wiley.com/10.1002/jor.23053.

[72] **Jha, S.C.**, **Fukuta, S.**, **Wada, K.**, **Higasino, K.**, **Amari-Kita, R.**, **Tsutsui, T. ... Sairyo, K.** (2016). Optimizing baseplate position in reverse total shoulder arthroplasty in small-sized Japanese females: Technical notes and literature review, *Journal of Medical Investigation*, *63*(1-2), 8–14.

[73] **Formaini, N.T.**, **Everding, N.G.**, **Levy, J.C.**, **Santoni, B.G.**, **Nayak, A.N.**, **Wilson, C. and Cabezas, A.F.** (2015). The effect of glenoid bone loss on reverse shoulder arthroplasty baseplate fixation, *Journal of Shoulder*

and Elbow Surgery, *24*(11), e312–e319, http://dx.doi.org/10.1016/j.jse.2015.05.045.

[74] **Rodríguez, J.A.**, **Entezari, V.**, **Iannotti, J.P. and Ricchetti, E.T.** (2019). Pre-operative planning for reverse shoulder replacement: the surgical benefits and their clinical translation, *Annals of Joint*, *4*, 4–4.

CURRICULUM VITAE

Name Surname: Majid Mohammad Sadeghi

EDUCATION:

- **B.Sc.:** 2005, Shahid Rajayee University, Department of Mechanical Engineering
- **M.Sc.:** 2011, Eastern Mediterranean University, Department of Mechanical Engineering

PUBLICATIONS, PRESENTATIONS AND PATENTS ON THE THESIS:

- **Mohammad Sadeghi, M.**, Kececi, E.F., 2020. Image Processing Methodology for Patient-Specific Instrument Design *International Journal of Medical Robotics and Computer Assisted Surgery*, doi:10.1002/rcs.2159, 2020
- Bilsel, K., Kapicioglu, M., Tezgel, O., **Mohammad Sadeghi, M.**, Kececi, E.F., Basaran, M.A., 2019. Effects of 3D Printed Patient Specific Guide Design for Shoulder Arthroplasty: An experimental study *29th Turkish National Congress of Orthopeadics and Traumatology*, 2019, Antalya, Turkey.
- **Mohammad Sadeghi, M.**, Kececi, E.F., Bilsel, K., and Aralasmak, A., 2018. Biomedical Image Processing Software Development for Shoulder Arthroplasty *Medical Image Processing for Improved Clinical Diagnosis*, Chapter 1. IGI Global. doi:10.4018/978-1-5225-5876-7, 2018
- **Mohammad Sadeghi, M.**, Kececi, E.F., Bilsel, K., and Aralasmak, A., 2018. Shoulder Surgery Accuracy Improvement with Image Processing *OMUZDIRSEK2018 10th Shoulder and Elbow Surgery Congress*, 2018, Ankara, Turkey.
- **Mohammad Sadeghi, M.**, Kececi, E.F., Bilsel, K., and Aralasmak, A., 2017. Biomedical Image Processing Software Development for Shoulder Arthroplasty: Shoulderart *CIBB 2017 Computational Intelligence Methods for Bioinformatics and Biostatistics*, 2017, Cagliari, Italy.
- **Mohammad Sadeghi, M.**, Kececi, E.F., Bilsel, K., and Aralasmak, A., 2017. Finding Glenoid Surface on Scapula in 3D Medical Images for Shoulder Joint Implant Operation Planning *ICMV 9th International Conference on Machine Vision*, doi:10.1117/12.2268409, 2016, Nice, France.

OTHER PUBLICATIONS, PRESENTATIONS AND PATENTS:

- Karagoz, Y., **Mohammad Sadeghi, M.**, 2018. Electronic Control Unit Development And Emissions Evaluation For Hydrogen-Diesel Dual Fuel Engines *Advances in Mechanical Engineering*, doi:10.1177/1687814018814076, 2018

- **Mohammad Sadeghi, M.**, and Kececi, E.F., 2018. Off-the-Shelf Electronics in Rescue Robotics *ICMSCE 2018 Mechatronics Systems and Control Engineering*, doi:10.1145/3185066.3185072, 2018, Amsterdam, Netherlands

- **Mohammad Sadeghi, M.**, and Kececi, E.F., 2016. Hybrid Power System for Mobile Robotics *ICPES 6th International Conference on Power and Energy Systems*, doi:10.1109/ICSRS.2016.7815839 2016, Paris, France.

- **Mohammad Sadeghi, M.**, and Kececi, E.F., 2016. Electronics of a Holonomic Rescue Robot with a Screw Drive Mechanism for Soft Terrain Mobility *ICAT 3rd International Conference on Advanced Technology and Sciences*, 2016, Konya, Turkey.

- **Mohammad Sadeghi, M.**, Kuduzoglu, M., and Kececi, E.F., 2014. An Open Software Open Hardware Hexapod Robot Platform for Robotic Education *TORK 2014, Turkish Autonomous Robots Conference*, 2014, Ankara, Istanbul

- Kuduzoglu, M., **Mohammad Sadeghi, M.**, and Kececi, E.F., 2014. Determination of Design Criteria for a Portable Urban Bomb Disposal Robot *TORK 2014, Turkish Autonomous Robots Conference*, 2014, Konya, Turkey.